U.S. Army
Research Institute of
Environmental Medicine
Natick, Massachusetts

TECHNICAL REPORT NO. T19-11
DATE May 2019

MODELING MALE TEMPERATURE PROFILES WITH THE FINITE ELEMENT METHOD AND ANATOMICALLY CORRECT HUMAN TORSOS

United States Army
Medical Research & Materiel Command

DISCLAIMER

The opinions or assertions contained herein are the private views of the author(s) and are not to be construed as official or reflecting the views of the Army or the Department of Defense. The investigators have adhered to the policies for protection of human subjects as prescribed in 32 CFR Part 219, Department of Defense Instruction 3216.02 (Protection of Human Subjects and Adherence to Ethical Standards in DoD-Supported Research) and Army Regulation 70-25.

USARIEM TECHNICAL REPORT T19-11

Modeling Male Temperature Profiles with the Finite Element Method and Anatomically Correct Human Torsos

Michael P.G. Castellani
Timothy P. Rioux
Adam W. Potter
Xiaojiang Xu

Biophysics and Biomedical Modeling Division

May 2019

U.S. Army Research Institute of Environmental Medicine
Natick, MA 01760-5007

REPORT DOCUMENTATION PAGE

Form Approved
OMB No. 0704-0188

PLEASE DO NOT RETURN YOUR FORM TO THE ABOVE ADDRESS.

1. REPORT DATE *(DD-MM-YYYY)*	2. REPORT TYPE	3. DATES COVERED *(From - To)*
22-05-2019	Technical Report	2018-2019

4. TITLE AND SUBTITLE

Modeling Male Temperature Profiles with the Finite Element Method and Anatomically Correct Human Torsos

5a. CONTRACT NUMBER

5b. GRANT NUMBER

5c. PROGRAM ELEMENT NUMBER

6. AUTHOR(S)

Michael P. Castellani
Timothy P. Rioux
Adam W. Potter
Xiaojiang Xu

5d. PROJECT NUMBER

5e. TASK NUMBER

5f. WORK UNIT NUMBER

H

7. PERFORMING ORGANIZATION NAME(S) AND ADDRESS(ES)

Biophysics and Biomedical Modeling Division
U.S. Army Research Institute of Environmental Medicine
Building 42 - 10 General Greene Ave
Natick, MA 01760

8. PERFORMING ORGANIZATION REPORT NUMBER

9. SPONSORING/MONITORING AGENCY NAME(S) AND ADDRESS(ES)

U.S. Army Medical Research and Materiel Command,
Fort Detrick, MD 21702

10. SPONSOR/MONITOR'S ACRONYM(S)

11. SPONSOR/MONITOR'S REPORT NUMBER(S)

T19-11

12. DISTRIBUTION/AVAILABILITY STATEMENT

Approved for public release; distribution unlimited

13. SUPPLEMENTARY NOTES

14. ABSTRACT

This paper demonstrates a novel approach in human thermoregulatory modeling. A male torso model was created from medical image data. This allowed for accurate geometry of the organs to be used when modeling thermoregulation. Thermoregulation was simulated through heat transfer using finite element analysis. The thermoregulatory activities consisted of vasodilation, vasoconstriction, sweating, and shivering. They all work together to attempt to create heat balance within the body.
The simulations show that temperature profiles and thermoregulatory responses can be predicted based on given the environmental conditions. In warm ambient temperatures, sweating and vasodilation occur in an attempt to exacerbate heat loss, while in cold ambient temperatures, shivering occurs to generate more heat and vasoconstriction occurs to lessen heat loss. The paths of the rectal and heart/esophageal temperatures compared well with similar temperatures recorded during previous studies, but the temperatures sometimes deviate significantly.

15. SUBJECT TERMS

thermal manikins; biophysics; clothing; predictive modeling; thermoregulation; headgear

16. SECURITY CLASSIFICATION OF:			17. LIMITATION OF ABSTRACT	18. NUMBER OF PAGES	19a. NAME OF RESPONSIBLE PERSON
a. REPORT	b. ABSTRACT	c. THIS PAGE			Adam W. Potter
Unclassified	Unclassified	Unclassified	Unclassified	55	19b. TELEPHONE NUMBER *(Include area code)* 508-233-4735

Reset

Standard Form 298 (Rev. 8/98)
Prescribed by ANSI Std. Z39.18

TABLE OF CONTENTS

LIST OF FIGURES

LIST OF TABLES

ACKNOWLEDGMENTS

The authors would like to thank Drs. Scott Montain and Samuel Cheuvront for their critical review and scientific discussions, and Drs. Andrew Spann and Nagi Elabbasi of Veryst Engineering LLC for their knowledge and expertise shared through consulting.

EXECUTIVE SUMMARY

This paper demonstrates a novel approach in human thermoregulatory modeling. A male torso model was created from medical image data. This allowed for accurate geometry of the organs to be used when modeling thermoregulation. Thermoregulation was simulated through heat transfer using finite element analysis. The thermoregulatory activities consisted of vasodilation, vasoconstriction, sweating, and shivering. They all work together to attempt to create heat balance within the body.

The simulations show that temperature profiles and thermoregulatory responses can be predicted based on given the environmental conditions. In warm ambient temperatures, sweating and vasodilation occur in an attempt to exacerbate heat loss, while in cold ambient temperatures, shivering occurs to generate more heat and vasoconstriction occurs to lessen heat loss. The paths of the rectal and heart/esophageal temperatures compared well with similar temperatures recorded during previous studies, but the temperatures sometimes deviate significantly.

LIST OF ABBREVIATIONS

Abbreviations are listed below with descriptions and units of each variable.

Table 1: list of each variable, their unit, and a description used throughout this paper

nomenclature	unit	description
BSA	m^2	body surface area
c_m	$m^3 \cdot s^{-1} \cdot m^{-3} \cdot W^{-1}$	proportionality coefficient
C_p	$J \cdot kg^{-1} \cdot K^{-1}$	specific heat at constant pressure
$C_{p,b}$	$J \cdot kg^{-1} \cdot K^{-1}$	specific heat at constant pressure of blood
$cold$	°C	output from cold receptors compared to set point
$cold_s$	°C	output from cold skin receptors compared to set point
dil	$L \cdot h^{-1}$	dilation value of blood vessels in skin
E_{calc}	$W \cdot m^{-2}$	calculated normal heat flux from sweat
E_{dif}	$W \cdot m^{-2}$	normal heat flux from diffusion
$E_{\max amb}$	$W \cdot m^{-2}$	maximum sweat heat flux that is physically possible
$E_{max\ sweat}$	$W \cdot m^{-2}$	maximum sweat heat flux that is physiologically possible
E_{reg}	$W \cdot m^{-2}$	normal heat flux from sweat production
E_{sweat}	$W \cdot m^{-2}$	normal heat flux from sweat
$error$	°C	average temperature difference from set point
h_c	$W \cdot m^{-1} \cdot K^{-1}$	convection coefficient
h_e	$W \cdot m^{-1} \cdot Pa^{-1}$	evaporative coefficient
h_r	$W \cdot m^{-1} \cdot K^{-1}$	radiative coefficient
LH	$J \cdot g^{-1}$	latent heat
LR	$K \cdot pa^{-1}$	Lewis ratio
M	W	metabolic heat produced
$M_{exercise}$	W	metabolic heat produced through exercise
M_{shiver}	W	metabolic heat produced through shivering
M_{tot}	W	total metabolic heat produced
P_a	Pa	ambient vapor pressure
P_{sk}	Pa	skin vapor pressure
q_n	$W \cdot m^{-2}$	heat flux in the normal direction
Q_0	$W \cdot m^{-3}$	basal metabolic rate per unit volume
Q_{shiver}	$W \cdot m^{-3}$	shivering metabolic rate
RH	%	relative humidity
R_{resp}	W	heat loss through the respiratory system
$stric$	1	vasoconstriction value of blood vessels in skin
$SweatRate_{max}$	$g \cdot s^{-1}$	the maximum sweat rate physiologically allowed

T	°C	temperature
T_a	°C	ambient temperature
T_b	°C	blood temperature
T_{body}	°C	average body temperature
T_{body_0}	°C	basal average body temperature
T_h	°C	average heart temperature
T_{h_0}	°C	basal average heart temperature
T_s	°C	average skin temperature
T_{s_0}	°C	basal average skin temperature
v_{air}	$m \cdot s^{-1}$	air velocity
V_b	L	volume of blood
V_{body}	L	volume of the torso
V_{muscle}	L	volume of the muscle
$warm$	°C	output from warm receptors compared to set point
$warm_s$	°C	output from warm shin receptors compared to set point
$\%BF$	%	percent body fat
λ	$W \cdot m^{-1} \cdot K^{-1}$	thermal conductivity
ω	$m^3 \cdot s^{-1} \cdot m^{-3}$	blood flow rate
ω_{muscle}	$m^3 \cdot s^{-1} \cdot m^{-3}$	muscle blood flow rate
ω_{muscle_0}	$m^3 \cdot s^{-1} \cdot m^{-3}$	basal muscle blood flow rate
ω_s	$m^3 \cdot s^{-1} \cdot m^{-3}$	skin blood flow rate
ω_{s_0}	$m^3 \cdot s^{-1} \cdot m^{-3}$	basal skin blood flow rate
$\omega_{s,calc}$	$m^3 \cdot s^{-1} \cdot m^{-3}$	total blood flow rate
Ω	$m^3 \cdot s^{-1}$	total blood flow rate
$\Omega_{s,calc}$	$m^3 \cdot s^{-1}$	skin blood flow rate
ρ	$kg \cdot m^{-3}$	density
ρ_b	$kg \cdot m^{-3}$	density of blood

INTRODUCTION

Models attempting to simulate thermoregulation have been developed and applied since the 1960s [1-3]. Simple geometries, such as cylinders and spheres, have been used to approximate the human body [2, 4-6]; however, these approximations do not truly capture the complex geometries of the human body. Medical image data can now be used to create an accurate representation of the human body. Finite element analysis can be used to simulate thermoregulation through heat transfer of the human body.

Body heat is transferred throughout the body by conduction, convection, radiation, and evaporation. Conduction occurs within and between the organs. Convection via blood flow is carried out through the blood to the organs. Convection also occurs between the boundary of the skin/clothing and the ambient environment. Radiation also occurs between the skin/clothing and the ambient environment. Evaporation is a thermoregulatory process occurs when liquid sweat vaporizes at the skin surface.

The body can also try and regulate heat flow to the environment by increasing or decreasing blood flow to the skin. Vasodilation is the increasing of the skin blood flow when the body is hot and vasoconstriction is the decreasing of the skin blood flow when the body is cold. Human bodies can also shiver when cold. Shivering helps produce more heat so that the body can try and stay at a desired temperature.

A finite element model is made when a continuous geometry of an object is discretized into a finite amount of elements. The finite element model can then be used in simulations that approximate the heat equation over the finite element model. This allows us to obtain temperature profiles of the model geometry.

The purpose of this project was to develop a thermoregulatory model of a male human torso using finite element analysis. Simulations were performed to investigate the model for accuracy in predicting human temperature profiles. This model calculates the body temperature from heat transfer physics, heat producing organs, blood temperature, shivering, sweating, vasoconstriction, vasodilation, and skin and muscle blood flow. Thermal properties, blood flow, and heat production of each organ were taken into account when computing the simulations. The output of the simulations would be the temperature profiles and average organ temperatures.

METHODS

BODY GEOMETRY AND ANATOMY

The simulations take place on a geometry or mesh of human torsos received from Synopsys (Mountain View, CA). The geometry is anatomically correct because it was generated from medical image data. This mesh consists of the following organs/tissues:

- Skin

- Fat
- Muscle
- Bladder
- Intestine
- Stomach
- Kidneys
- Lungs
- Liver
- Heart
- Bones

Images of the geometries are shown in Figure 1, Figure 2, and Figure 3. The volume and mass of each organ are shown in Table 2. The geometry does not include any arteries or veins. This implies no blood flow is modeled (it is also computationally expensive to model fluids). The heat transfer between the tissue and blood are modeled with Eq. 1 and Eq. 26.

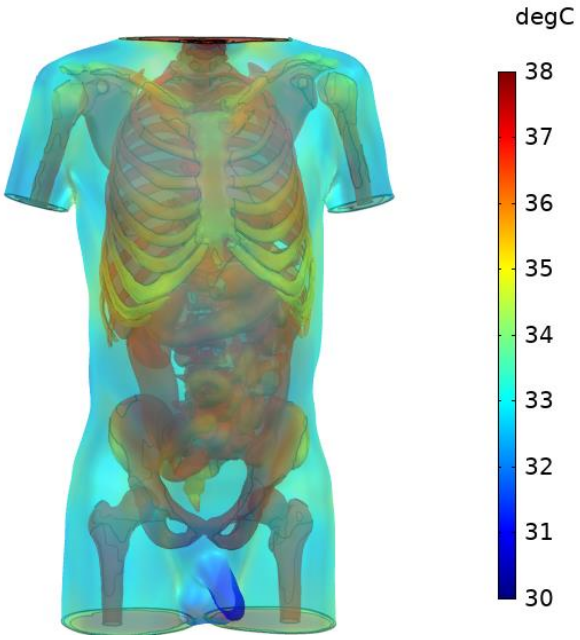

Figure 1: image of the torso model

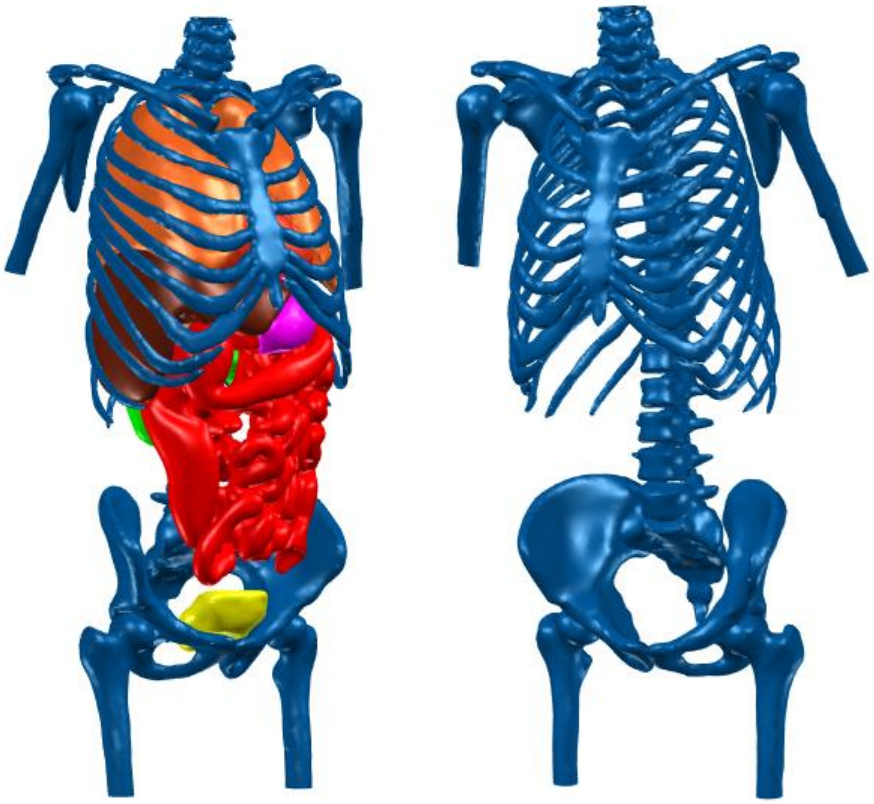

Figure 2: bones and internal organs of the torso meshes

Figure 3: torso muscle

Table 2: volume and mass of each organ

organ	volume (cm^3)	volume (%)	mass (kg)
skin	2518.4	5.41%	2.73
fat	14831	31.89%	13.65
muscle	17962	38.62%	19.49
bladder	172.7	0.37%	0.16
intestine	2074.6	4.46%	2.25
stomach	377.9	0.81%	0.36
kidneys	322.5	0.69%	0.35
lungs	2820.2	6.06%	1.58
liver	1842.2	3.96%	1.99
heart	770.23	0.15%	0.83
bones	3516.9	7.56%	4.77
total	46508.63	100%	48.16

BODY BIOPHYSICAL PROPERTIES

Each organ was given specific thermal properties that were derived from literature. Table 3 displays each thermal property given to the organs. These thermal properties are thermal conductivity (λ), density (ρ), specific heat (C_p), blood flow rate (ω), and metabolic rate (Q). Each of these thermal properties help describe temperature variations within the body.

Table 3: thermal properties for each organ

organs	λ (W·m^{-1})	ρ (kg·m^{-3})	C_p (J·kg^{-1}·K^{-1})	Q_0 (W·m^{-3})	ω_0 (m^3·s^{-1}·m^{-3})
skin	0.47	1085	3680	368.12	3.61E-04
fat	0.21	920	2300	368.36	7.70E-05
muscle	0.51	1085	3800	684.18	5.42E-04
bladder	0.48	930	3200	370.37	1.54E-04
intestine	0.47	1085	3200	368.34	6.40E-03
stomach	0.51	960	3560	368.34	6.40E-03
kidneys	0.48	1080	3600	23889	7.20E-02
lungs	0.28	560	3520	365.49	2.95E-02
liver	0.48	1080	3690	14413.6	1.80E-02
heart	0.47	1080	3550	24000	1.08E-01
bones	0.75	1357	1700	368.32	0

HEAT BALANCE EQUATION

Heat transfer physics is governed by the heat equation, which states

$$\rho C_p \frac{\partial T}{\partial t} = \lambda \nabla^2 T + Q_0 + Q_{exercise} + Q_{shiver} + \omega \rho_b C_{p,b}(T_b - T) \qquad \text{Eq. 1}$$

where ρ is the density (kg·m^{-3}), C_p is the specific heat (J·kg^{-1}·K^{-1}), T is temperature (°C), t is time (s), ∂ is the symbol for partial derative, λ is the thermal conductivity (W·m^{-1}), ∇ is the gradient, Q_0 is the basal metabolic rate (W·m^{-3}), $Q_{exercise}$ is the exercise metabolic rate (W·m^{-3}), Q_{shiver} is the metabolic rate due to shivering (W·m^{-3}), ω is the blood flow rate (m^3·s^{-1}·m^{-3}), ρ_b is the density of blood, $C_{p,b}$ is the specific heat of blood, and T_b is the temperature of blood.

Boundary conditions

In these particular models, the heat transfer from the skin to the environment occurs from convection, radiation, and evaporation. This was modeled as

$$q_n = h_c(T - T_a) + h_r(T - T_r) + E_{sweat} \qquad \text{Eq. 2}$$

where q_n is the heat flux normal to the boundary (W·m^{-2}), h_c is the convection coefficient (W·m^{-2}·K^{-1}), T is the temperature (°C) T_a is the ambient temperature (°C), h_r

is the radiation coefficient ($W \cdot m^{-2} \cdot K^{-1}$), T_r is the radiative temperature of the environment, and E_{sweat} is the heat flux caused by sweat evaporation ($W \cdot m^{-2}$). The convective coefficient was calculated by [7]

$$h_c = 2.7 + 8.7 v_{air}^{0.67} \quad \text{Eq. 3}$$

where v_{air} is the wind speed ($m \cdot s^{-1}$). Typically, h_r is a third degree polynomial depending on temperature, but assuming a constant value of 4.5 $W \cdot m^{-2} \cdot K^{-1}$ was deemed acceptable for this application [1]. Heat loss from evaporation is explained in the thermoregulation section.

Initial Conditions

For dynamic simulations, the initial conditions of the model at rest in a static thermal neutral condition are T_a = 28°C, v_{air} = 0.4 $m \cdot s^{-1}$, and relative humidity (RH) = 0.4.

THERMOREGULATION

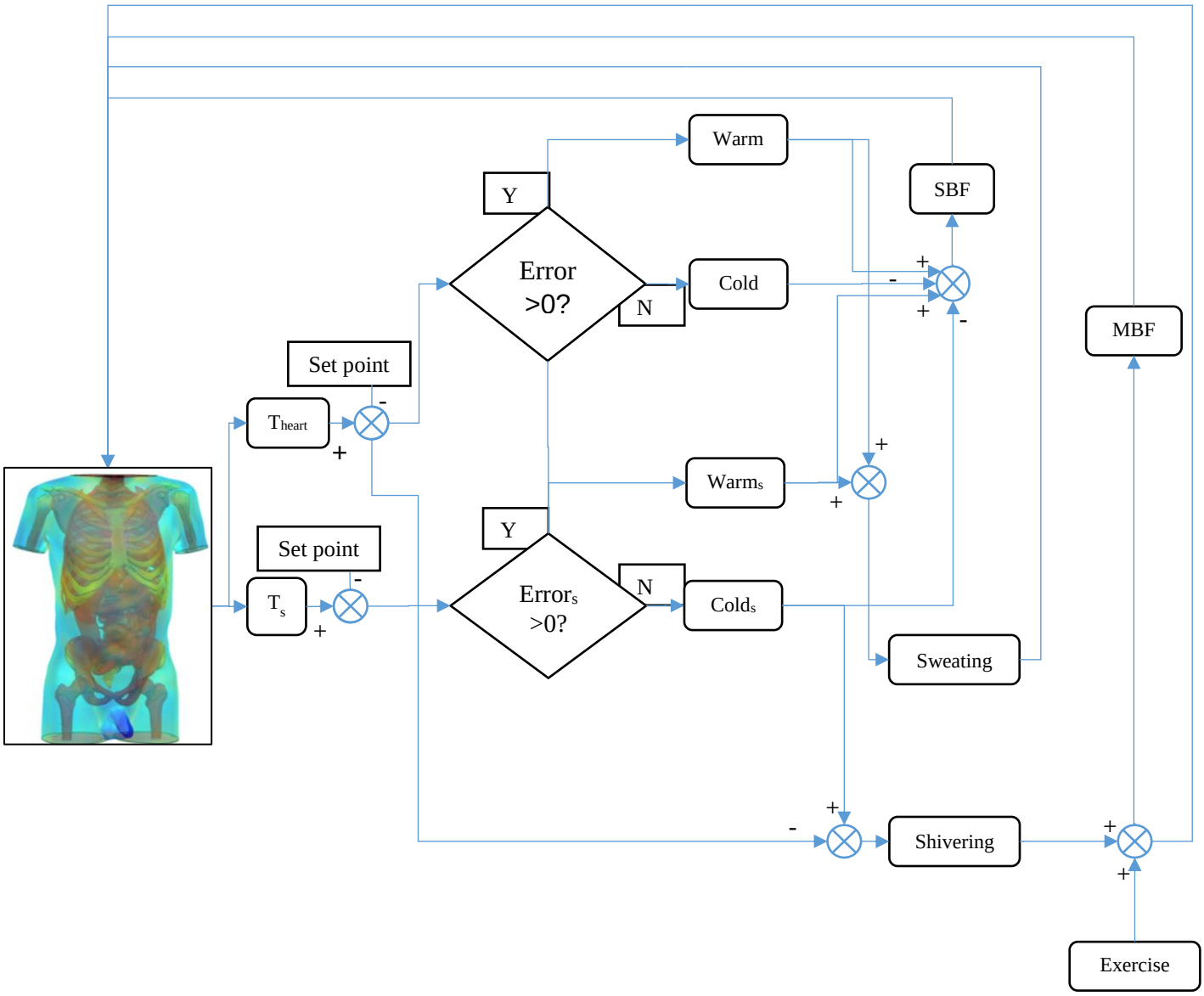

Figure 4: Thermoregulatory control system

Figure 4 shows the thermoregulatory model. The control signal is from the heart and skin temperatures. Error is calculated by Eq. 4. Error_s is calculated by Eq. 7. Warm and Warm_s are calculated by Eq. 5 and Eq. 8 respectively. Cold and Cold_s are calculated by Eq. 6 and Eq. 9 respectively. Skin blood flow (SBF) is calculated with Warm, Cold, Warm_s, and Cold_s. First, values for vasodilation and vasoconstriction are calculated. Then, those values are used to calculate the change in SBF. Sweating is a function of Warm and Warm_s. Shivering is a function of Cold_s and Error. Shivering and Exercise both change the muscle blood flow (MBF). SBF, Sweating, Shivering, MBF, and Exercise all affect the heat transfer in the torso and the process is repeated.

This model treats the human body as a control system [8]. Here the torso attempts to return to equilibrium temperature by changing its blood flow, shivering, and sweating. The deviation or error from the desired body temperature is defined to be:

$$error = T_h - T_{h_0} + 0.01\frac{dT_h}{dt} \quad \text{Eq. 4}$$

Here $error$ is the difference from equilibrium where the time derivative is incorporated (°C), T_h is the average temperature of the heart (°C), and T_{h_0} is the average temperature of the heart in thermal neutral conditions (°C). $\frac{dT_h}{dt}$ is the rate of temperature change of the heart (°C·s^{-1}). Warmth and coldness of the heart were then defined as [8]

$$warm = \begin{cases} error, & error > 0 \\ 0, & error \leq 0 \end{cases} \quad \text{Eq. 5}$$

$$cold = \begin{cases} -error, & error < 0 \\ 0, & error \geq 0 \end{cases} \quad \text{Eq. 6}$$

where $warm$ and $cold$ are measured in °C. The error in the skin temperature was also measured. This was defined as

$$error_s = T_s - T_{s_0} \quad \text{Eq. 7}$$

Here $error_s$ is the difference from the equilibrium skin temperature (°C), T_s is the average skin temperature (°C), and T_{s_0} is the average skin temperature in thermal neutral conditions (°C). The warmth and coldness of the skin are also defined as [8]

$$warm_s = \begin{cases} error_s, & error_s > 0 \\ 0, & error_s \leq 0 \end{cases} \quad \text{Eq. 8}$$

$$cold_s = \begin{cases} -error_s, & error_s < 0 \\ 0, & error_s \geq 0 \end{cases} \quad \text{Eq. 9}$$

where $warm_s$ and $cold_s$ are measured in °C.

Vasodilation/Vasoconstriction

Vasodilation and vasoconstriction of the skin help the body expel or retain heat. The value of vasodilation was calculated as [8]:

$$DIL = 117.0 * error + 7.5 * (warm_s - cold_s) \quad \text{Eq. 10}$$

where DIL is the increased blood flow ($L \cdot h^{-1}$). $DIL = 0$ when $DIL \leq 0$. Vasoconstriction was calculated as [8]:

$$STRIC = -5 * (error + warm_s - cold_s) \quad \text{Eq. 11}$$

where $STRIC$ is the value of vasoconstriction (1). $STRIC = 0$ when $STRIC \leq 0$. The total blood flow was then calculated as [8]:

$$\Omega_{s,calc} = \frac{\int \omega_{s_0} dV_s + 0.161 * \frac{DIL}{3600}}{1 + 0.2 * STRIC} 2^{\frac{error}{10}} \quad \text{Eq. 12}$$

where $\Omega_{s,calc}$ is the calculated blood flow rate of the skin ($m^3 \cdot s^{-1}$), ω_{s_0} is the blood flow rate of the skin in thermal neutral conditions ($m^3 \cdot s^{-1} \cdot m^{-3}$), and V_s is the volume of the skin (L). DIL was divided by 3600 to convert the unit from $L \cdot h^{-1}$ to $L \cdot s^{-1}$. The calculated skin blood flow,$\omega_{s,calc}$ ($m^3 \cdot s^{-1} \cdot m^{-3}$) is then calculated by

$$\omega_{s,calc} = \frac{\Omega_{s,calc}}{V_s} \quad \text{Eq. 13}$$

where V_s is the volume of the skin (m^3). An upper bound of $10\omega_{s_0}$ was placed on the blood flow rate. The blood flow rate of the skin was then calculated as

$$\omega_s = \min\{\omega_{s,calc}, 10\omega_{s_0}\} \quad \text{Eq. 14}$$

Where ω_s is the blood flow rate of the skin ($m^3 \cdot s^{-1} \cdot m^{-3}$). The $\min\{\}$ is used to take the minimum of $\omega_{s,calc}$ and $10\omega_{s_0}$. That way, if $\omega_{s,calc}$, the calculated blood flow rate exceeds $10\omega_0$ then $\omega_s = 10\omega_0$. The $10\omega_0$ is a generous upper limit for skin blood flow [9].

Sweating

The calculated amount of heat loss from sweat was calculated by [7]

$$E_{calc} = E_{dif} + E_{reg} \quad \text{Eq. 15}$$

where E_{calc} is the calculated heat loss ($W \cdot m^{-2}$), E_{dif} is the heat loss from diffusion ($W \cdot m^{-2}$), and E_{reg} is the heat loss from secreted sweat ($W \cdot m^{-2}$). E_{dif} was assumed to be 10 $W \cdot m^{-2}$. E_{reg} was calculated by

$$E_{reg} = \frac{352 * error + 32(warm_s - cold_s)}{1.8877} \quad \text{Eq. 16}$$

The original equation by Stolwijk and Hardy calculated the heat loss in W. To change the units to W·m^{-2}, E_{reg} calculated from Eq. 16 was divided by the surface area of their model, 1.8877 m^2.

Upper limits on the amount of sweating were also calculated. $E_{\max sweat}$, the maximum heat loss from the upper bound of sweating that is physiologically possible (W·m^{-2}) was calculated by

$$E_{\max sweat} = \frac{SweatRate_{max} * LH}{BSA} \quad \text{Eq. 17}$$

Where $SweatRate_{max}$ is the maximum possible sweat rate (g·s^{-1}), LH is the latent heat of evaporation of water (J·g^{-1}), and BSA is body surface area (m^2). $SweatRate_{max}$ was set to 0.5 g·s^{-1} [7]. LH is 2264 J·g^{-1}. The maximum evaporative heat loss that would be possible due to the maximum pressure gradient was also calculated and used as an upper bound.

$$E_{\max amb} = h_e(P_{sk} - P_a) \quad \text{Eq. 18}$$

Where $E_{\max amb}$ (W·m^{-2}) is the maximum heat loss due to the pressure gradient, h_e is the evaporative coefficient (W·m^{-1}·Pa^{-1}), P_{sk} is the pressure at the skin (Pa), and P_a is the pressure from the ambient environment (Pa). h_e was calculated by

$$h_e = LR * h_c \quad \text{Eq. 19}$$

Where LR is the Lewis relation (K·Pa^{-1}) and h_c is the convective coefficient (W·m^{-2}·K^{-1}). Here LR was set to $16.5 * 10^{-3}$ K·Pa^{-1} [1]. P_{sk} (Pa) and P_a (Pa) are calculated by [10]:

$$P_{sk} = 100 * e^{18.965 - \frac{4010}{235 + T_s}} \quad \text{Eq. 20}$$

$$P_a = RH * 100 * e^{18.965 - \frac{4010}{235 + T_a}} \quad \text{Eq. 21}$$

Here T_s is the average skin temperature (°C), T_a is the ambient temperature (°C), and RH is the relative humidity (decimal). The heat loss from sweat is chosen by:

$$E_{sweat} = \min\{E_{calc}, E_{\max sweat}, E_{max\ amb}\} \quad \text{Eq. 22}$$

Where E_{sweat} is the heat loss from sweat (W·m^{-2}). The $\min\{\ \}$ function is used to take the minimum of E_{calc}, $E_{\max sweat}$, and $E_{max\ amb}$, which will prevent E_{sweat} from being greater than either the physiologically or physically possible upper bounds.

Shivering

Metabolic heat from shivering was calculated by [11]:

$$Q_{shiver} = 0.705 \frac{155.5 * (-error) + 47 * (-error_s) - 1.56 * (-error_s)^2}{\sqrt{\%BF}} \frac{BSA}{V_{muscle}} \quad \text{Eq. 23}$$

Where Q_{shiver} is the metabolic heat from shivering (W·m^{-3}), $\%BF$ is the percent body fat, BSA is the body surface area (m^2), and V_{muscle} is the volume of the torso muscle (m^3). The 0.705 was included because 70.5% of metabolic activity from shivering occurs in the torso [12]. $\frac{BSA}{V_{muscle}}$ was added to the equation because the initial equation by Xu et al had the units W·m^{-2}. Multiplying by the BSA produces the unit W, multiplying by 0.705 gives the heat produced by muscle in the torso, and dividing by V_{muscle} produces the metabolic heat source in the muscle from shivering in W·m^{-3}. An upper bound for shivering was set. This value was

$$Q_{shiver,max} V_{muscle} = 0.705 * 450 \quad \text{Eq. 24}$$

Where $Q_{shiver,max}$ is the upper bound for shivering (W·m^{-3}), V_{muscle} is the volume of the muscle. It is estimated that approximately 450 W is the most heat a human can produce from shivering [13]. This is multiplied by 0.705 to give the maximum amount of heat the torso could produce.

Muscle Blood Flow

When exercising, the blood flow to the muscles increases so that the demand for oxygen is met. This thermoregulatory event was modeled as [1]

$$\omega_{muscle} = \omega_{muscle_0} + c_m(M_{shiver} + M_{exercise}) \quad \text{Eq. 25}$$

Where ω_{muscle_0} is the basal blood flow rate of muscle (m^3·s^{-1}·m^{-3}), c_m is the proportionality coefficient (m^3·s^{-1}·m^{-3}·W^{-1}), M_{shiver} is the metabolic heat produced from shivering (W), and $M_{exercise}$ is the metabolic heat produced from exercise (W). The original equation only included $M_{exercise}$, but to our knowledge there is no information how shivering affects the blood flow to muscle so we assumed that each Watt of shivering has the same effect on muscle blood flow as each Watt of exercise. c_m was set to $1.546 * 10^{-5}$ m^3·s^{-1}·m^{-3}·W^{-1}.

Blood Temperature

Inside the body heat is mainly transferred from conduction and through the blood mostly by convection. Thus it is important that the blood temperature changes with respect to the heat gained from the organs or lost to the organs. This equation was modeled as [14]:

$$V_b \frac{\partial T_b}{\partial t} = \sum_{i=1}^{11} [\Omega_i (T_i - T_b)] - \frac{R_{resp}}{\rho_b C_{p,b}} \quad \text{Eq. 26}$$

Where V_b is the volume of the blood (m^3), T_b is the blood temperature (°C), i is the indexer for the 11 organs present, Ω is the blood flow rate of the 'ith' organ ($m^3 \cdot s^{-1}$), T_i is the average temperature of the 'ith' organ (°C), R_{resp} is the respiratory heat loss (W), ρ_b is the density of blood ($kg \cdot m^{-3}$), and $C_{p,b}$ is the specific heat of blood ($J \cdot kg^{-1} \cdot K^{-1}$). V_b was assumed to be 5 L (0.005 m^3). R_{resp} was calculated by [7]:

$$R_{resp} = 0.0014M_{tot}(34 - T_a) + 0.0173M_{tot}(5.87 - P_a * 10^{-3}) \quad \text{Eq. 27}$$

Where M_{tot} is the total metabolic heat produced (W), T_a is the ambient temperature (°C), and P_a is the ambient pressure (Pa). M_{tot} was calculated using METs because the entire body was not present. 1 MET is equivalent to 58.2 $W \cdot m^{-2}$ [7]. M_{tot} was then calculated by

$$M_{tot} = met * BSA + (Q_{shiver} + Q_{exercise})V_{muscle} \quad \text{Eq. 28}$$

Here BSA is the body surface area (m^2), Q_{shiver} is the metabolic heat source from shivering ($W \cdot m^{-3}$), $Q_{exercise}$ is the metabolic heat source from exercise ($W \cdot m^{-3}$), and V_{muscle} is the volume of the muscle (m^3).

COMSOL MULTIPHYSICS® IMPLEMENTATION

All simulations were performed using COMSOL Multiphysics® version 5.4. Under Global Definitions, constants and basal values were placed under parameter nodes (Figure 5). Functions were also placed under Global Definitions (Figure 5). To keep everything organized, “group by type” was turned on. Under Model 1 (mod1) one can find the integrations used (Figure 8), points used to approximate average temperatures, variables, and the ambient conditions. Integrations and average integrations were placed under Component Couplings. The label is the name of each coupling and in the parentheses is the operator name. For instance if someone would want the average temperature of the skin you would use aveop1() to denote average skin and T to denote temperature. You would type aveop1(T) to calculate the average temperature of the skin. Anatomic location points can be found under probes. Four skin points were used to calculate the average skin temperature. Variables (defined user values/expressions that can be non-uniform across space) are found under the variables node (Figure 6). Here you can create user-defined expressions, where one can build upon the parameters, functions, integrations/couplings, and points/probes. Directly under the variables node is a list of different groupings of variables. These variables consist of the ambient properties, clothing properties, and the thermoregulation functions. Ambient and clothing properties are under the first group. The next two nodes define the input variables and the deviation from thermal neutral. Then the skin blood flow is calculated. The next group consists of sweating. In the first node, the maximum amount of heat loss from sweat is calculated. Then, the heat loss from sweating is calculated. The next node calculates the metabolic heat source from shivering. Then, the heat loss from the respiratory rate is calculated. Then, the blood flow of each organ is calculated. Finally, the metabolic heat source of each organ is calculated. The nojac() function is used when calculating any thermoregulatory value. The nojac() function means that the thermoregulatory function will not be used in formulating the Jacobian. This is because the average temperatures used have a coupling effect and will overpopulate the Jacobian matrix using too much memory.

Under the Multiphysics branch, there exists an “Ambient Thermal Properties” node. This is where the ambient temperature is defined (Figure 7).

The Bioheat Transfer branch is where the heat transfer is applied to the torso. All parts are defined as biological tissue. Each organ receives a blood temperature, specific heat of blood, blood flow (perfusion) rate, density, and metabolic heat source (Figure 9). Blood temperature is defined under “Global Equations Blood” (Figure 10). The heat flux at any boundary that is not skin is set to 0. The heat flux from convection and radiation are defined next (Figure 11). The external temperature for convection is set to the ambient temperature and the external temperature for radiation is set to the user defined value of T_r. Next, the heat flux from evaporation is defined. Finally, the heat source when exercising is assigned to the muscle.

Simulations can take place once the physics is properly added (Figure 12). Due to the thermal regulation functions being non-linear, an iterative solver is used instead of

a direct solver. The Relative tolerance under the “Stationary Solver 1” is set to 1e-5. The default is 1e-3, however, it did not prove as reliable as 1e-5. Under “Fully Coupled 1” there exists a section called “Method and Termination.” Here the “Termination technique was changed from tolerance to iterations or tolerance and the “Number of iterations” was set to 50. This way no error would occur if the simulation did not converge to the specified amount. For any stationary problem, the solution that was previously outputted was set to be used as the initial solution if the simulation runs again. The first simulation to take place is a static simulation at thermal neutral. Initially thermoregulation was not included so that the basal temperature values of the skin and heart could be found. The values were then incorporated into COMSOL Multiphysics®. Now, any simulation desired could run and the thermoregulatory effects would be included. For time dependent simulations (Figure 13), the initial values given to the simulation is the solution from the thermal neutral simulation. Time steps were altered to try and minimize error in the calculations.

Figure 14 and Figure 15 show how results can be derived in COMSOL Multiphysics®. Figure 14 shows a 3D graph of the temperature throughout the torso. Figure 15 shows a table of values that are derived from the steady state simulation.

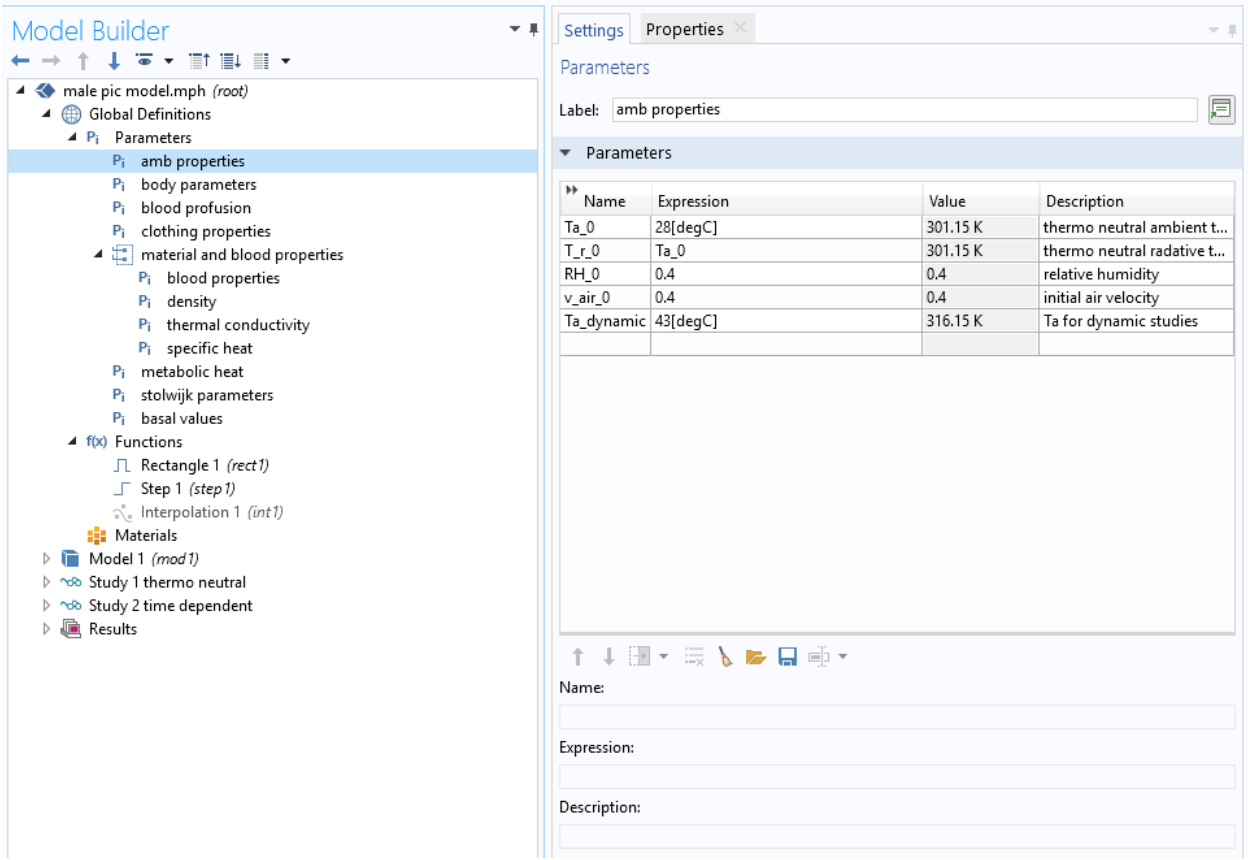

Figure 5: image of parameters

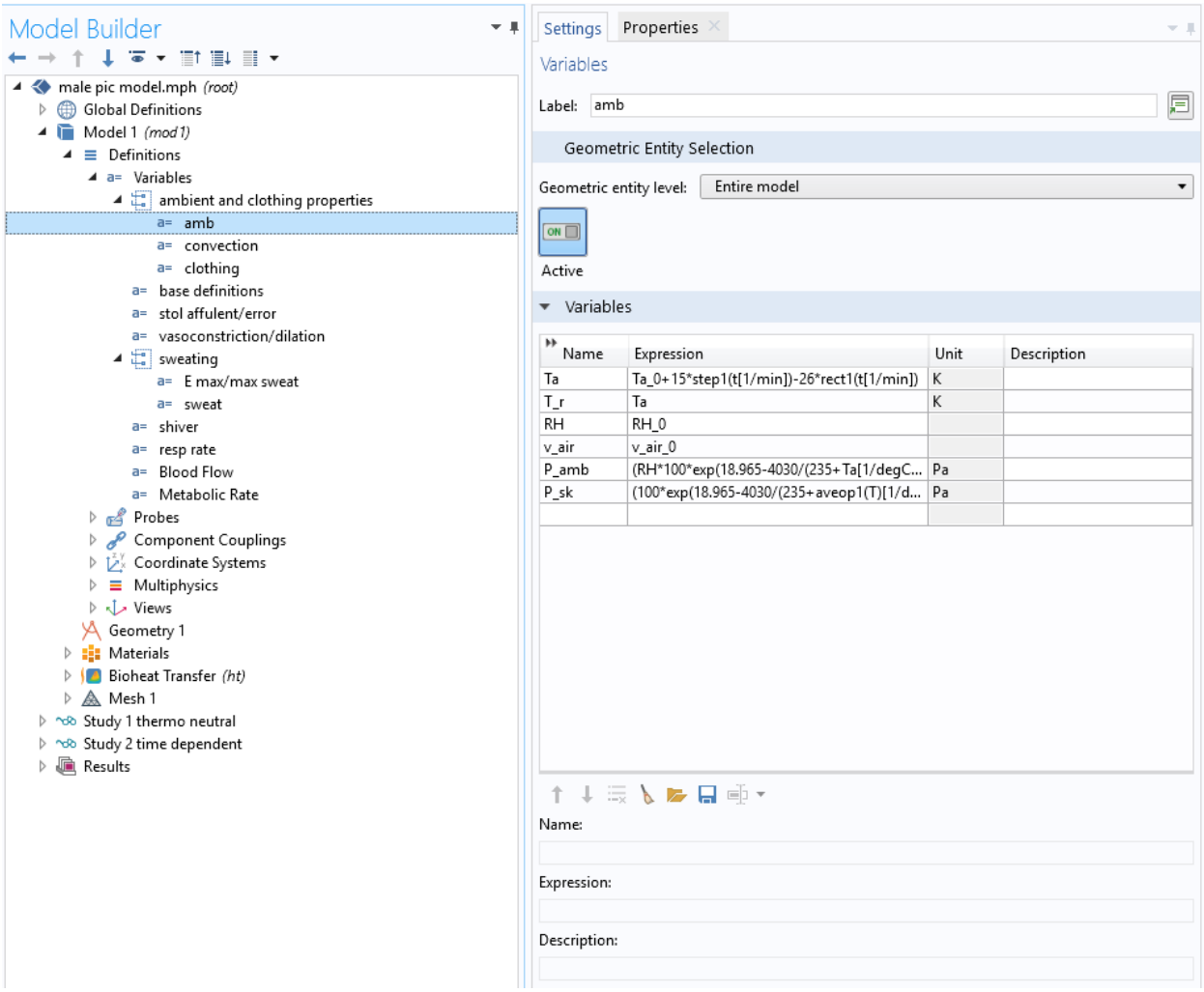

Figure 6: variables

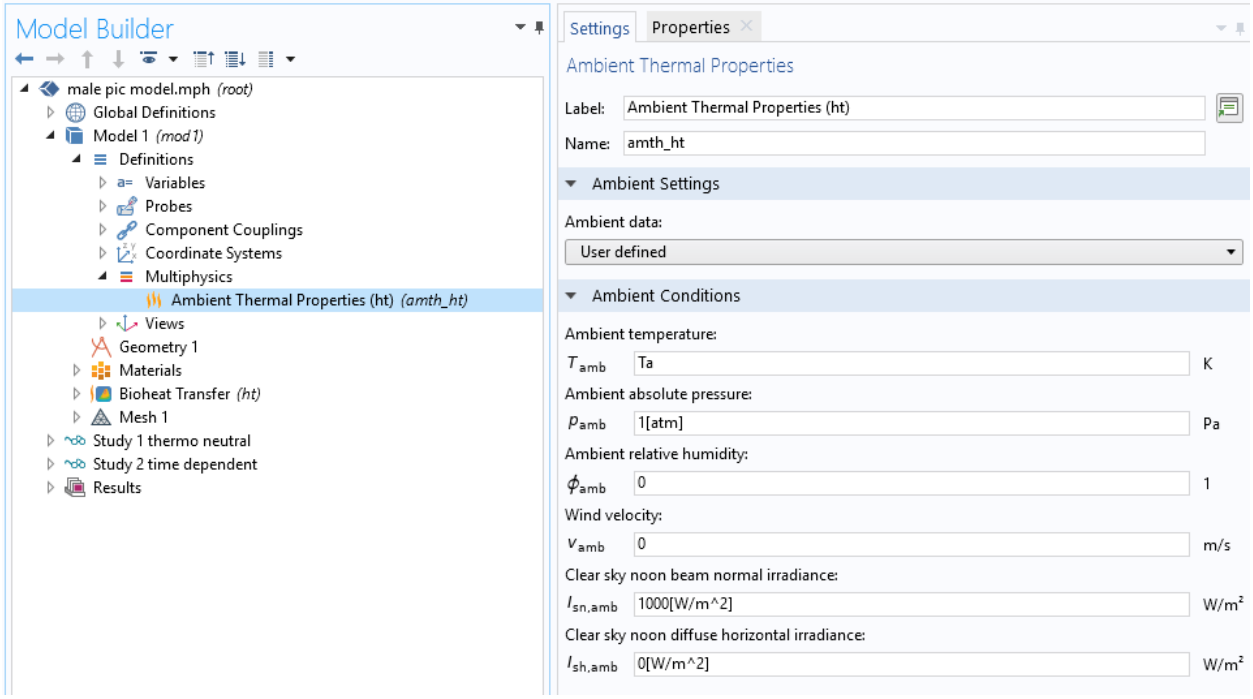

Figure 7: ambient properties

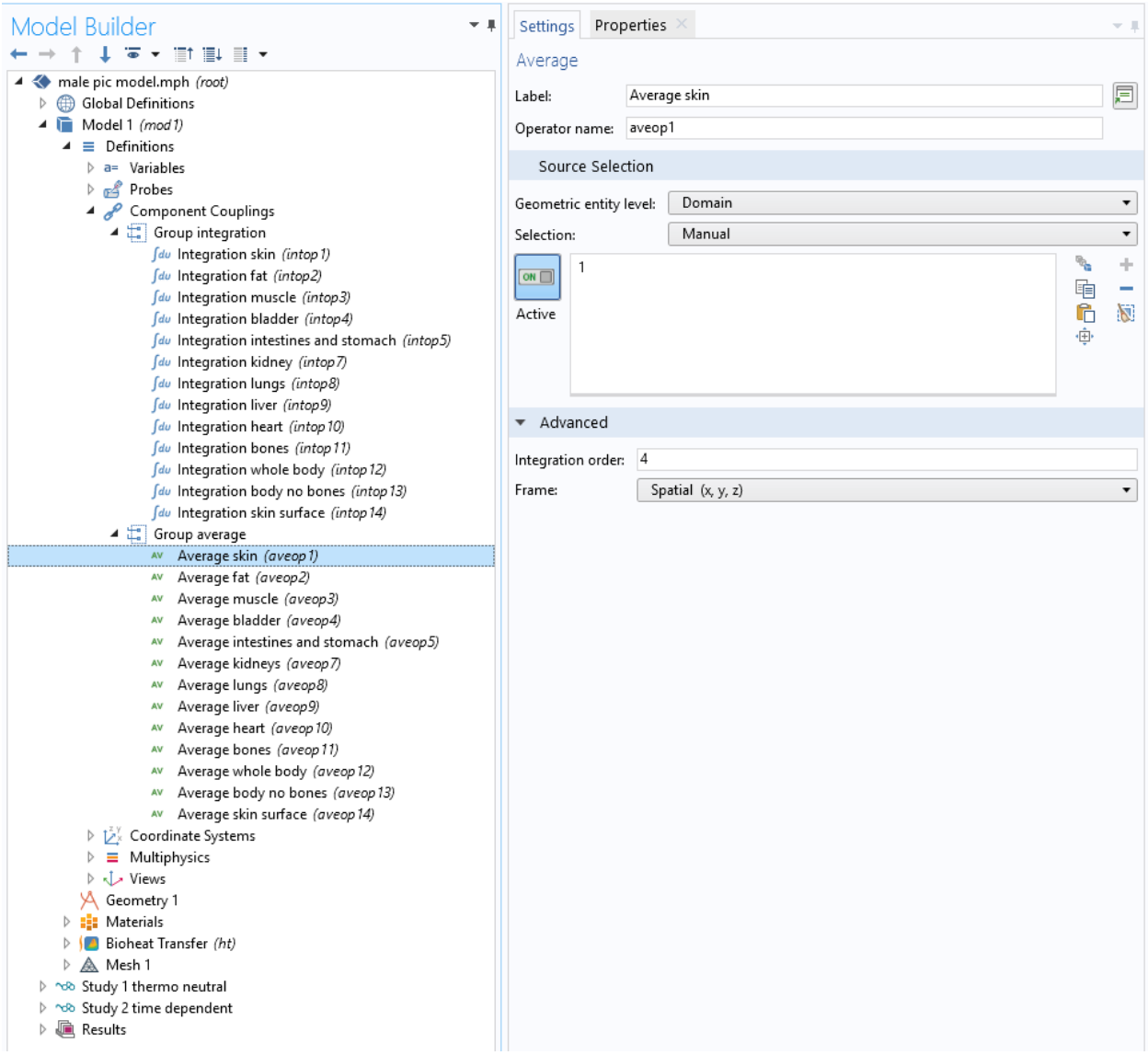

Figure 8: couplings

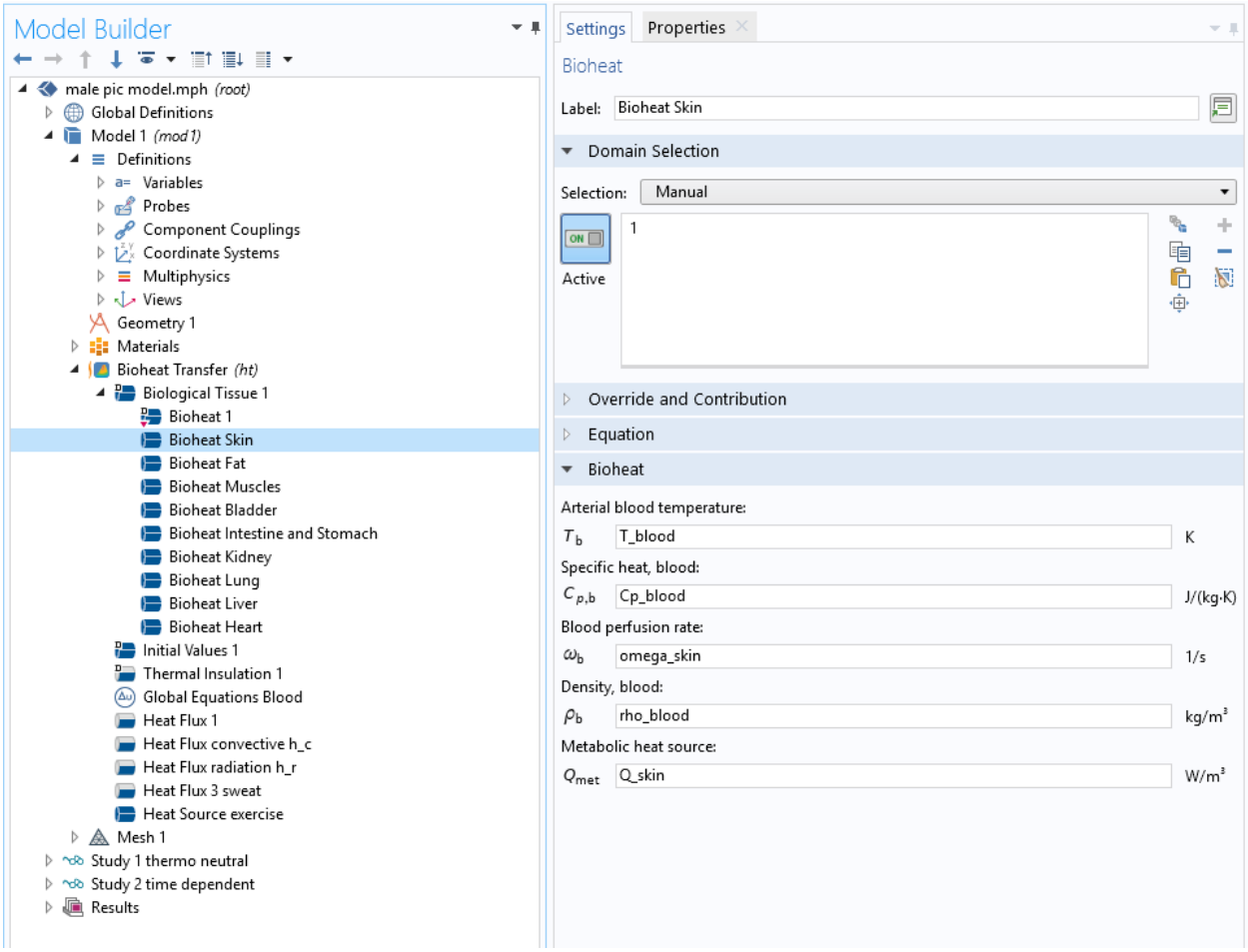

Figure 9: bioheat skin

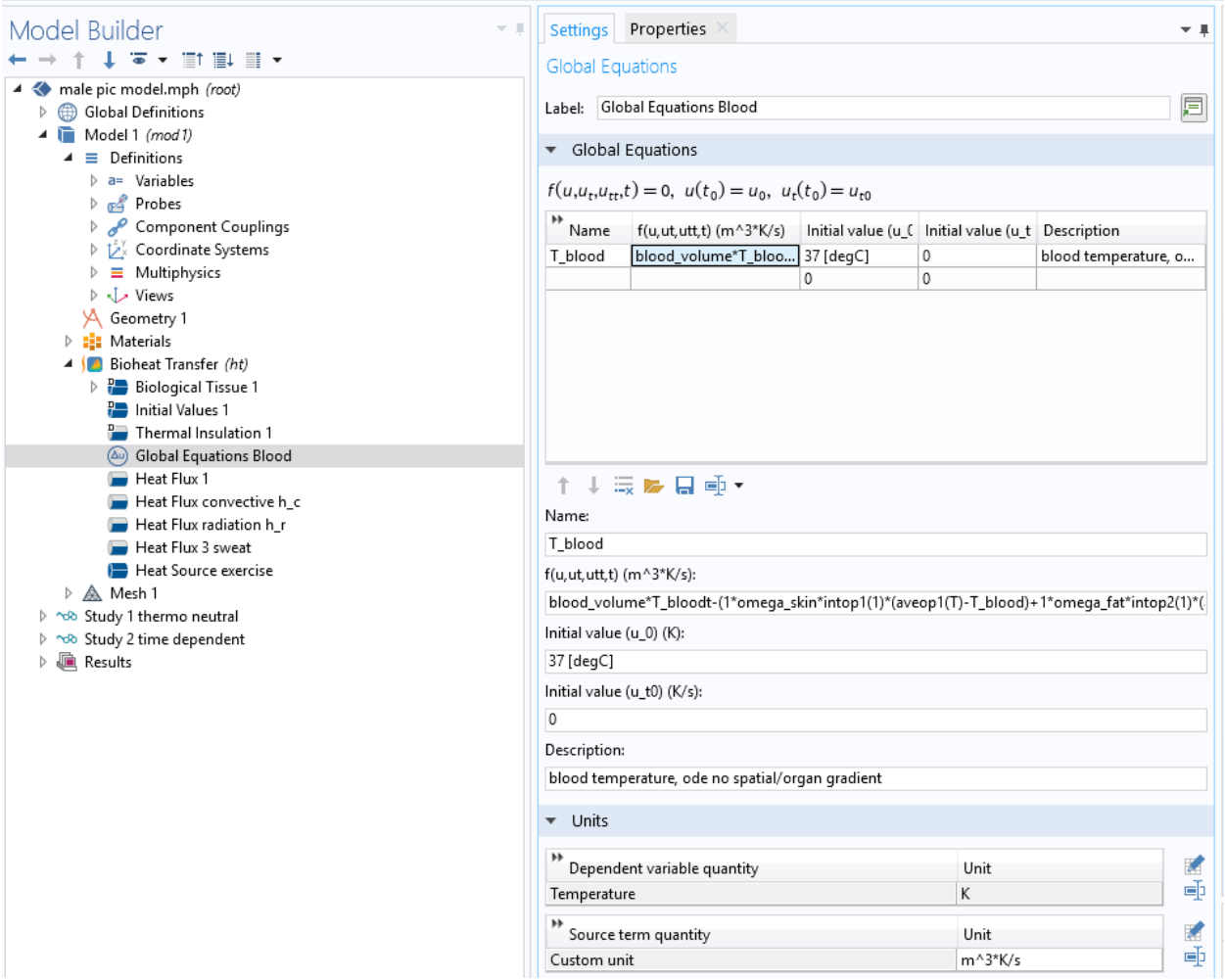

Figure 10: blood temperature equation

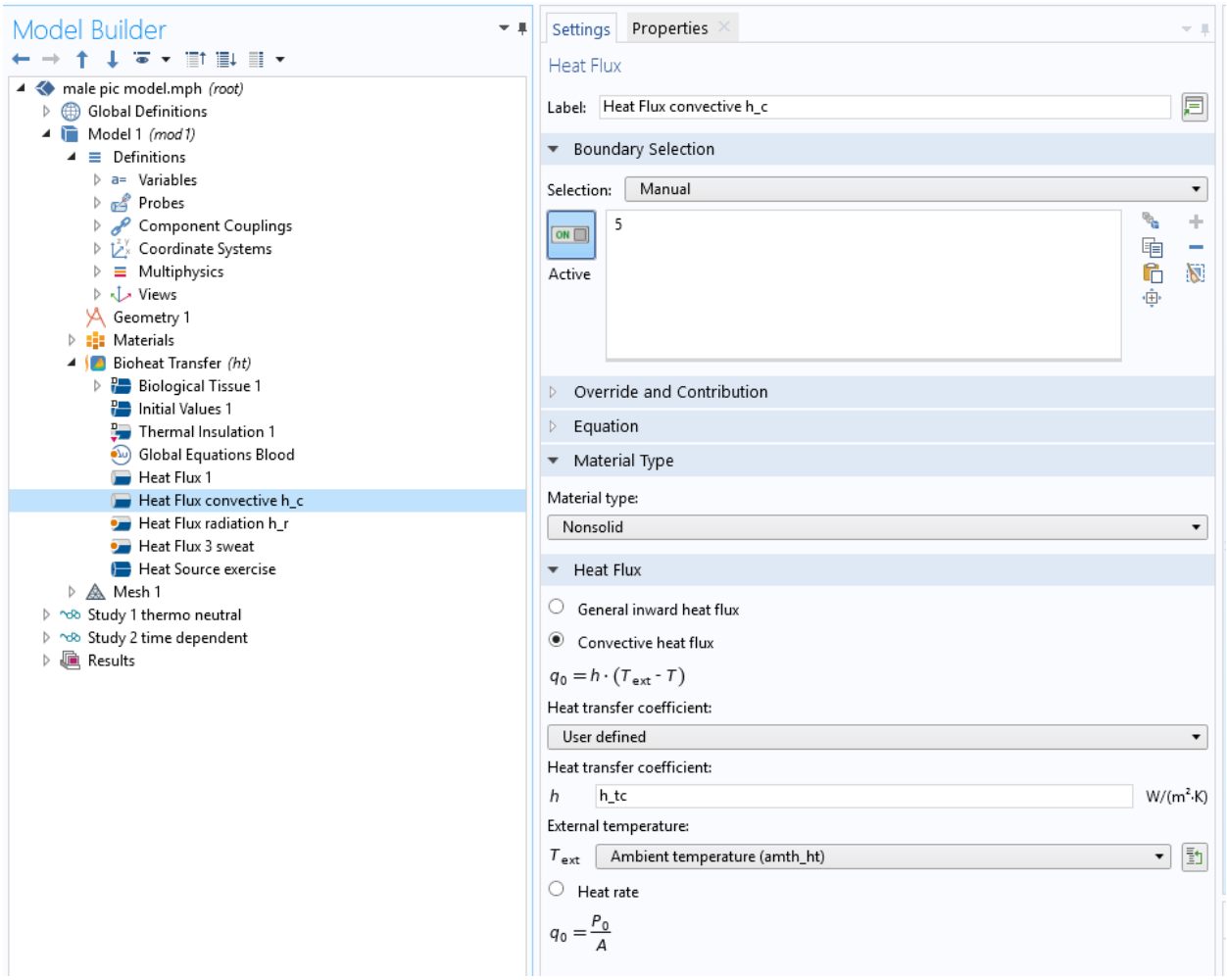

Figure 11: convective heat flux

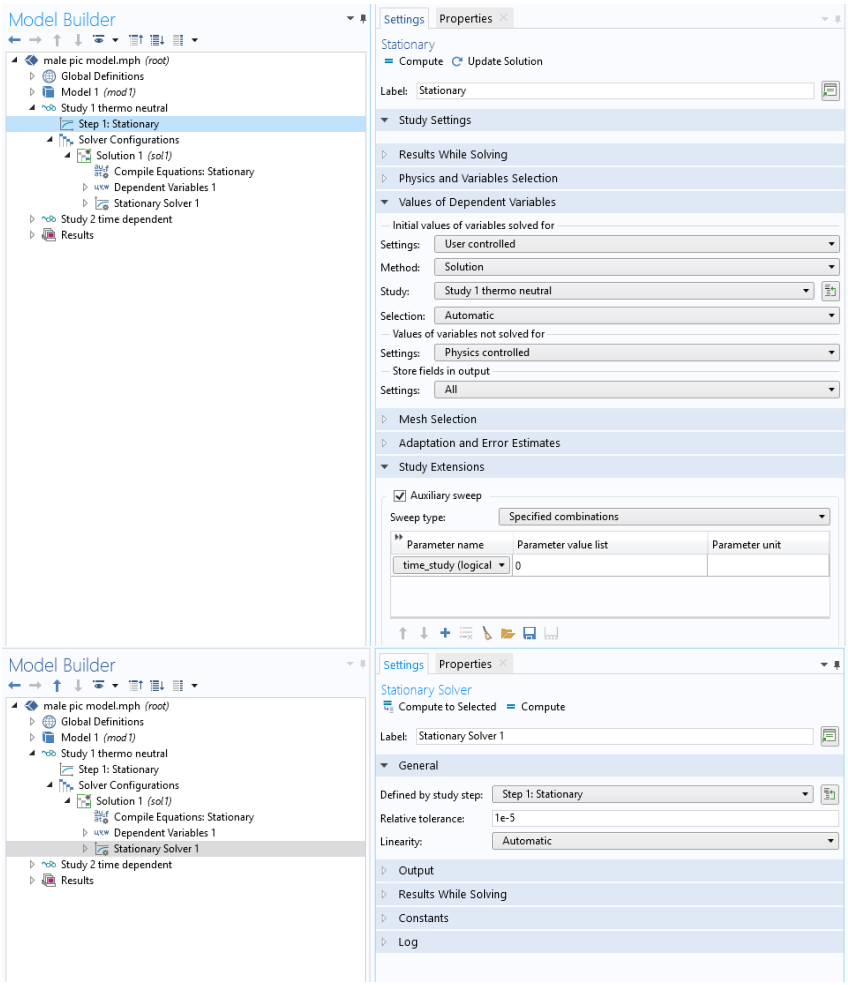

Figure 12: stationary simulation

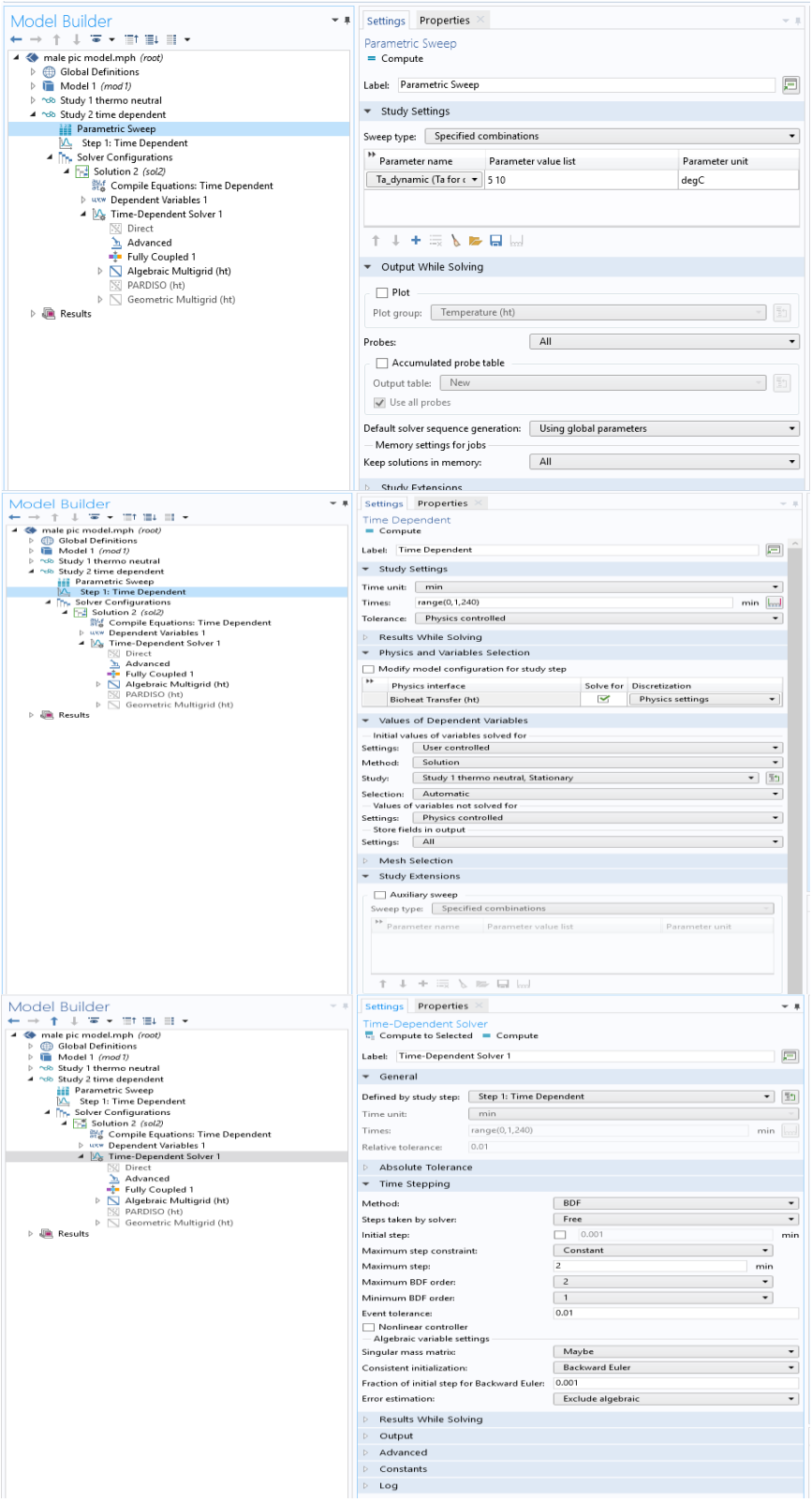

Figure 13: dynamic simulation

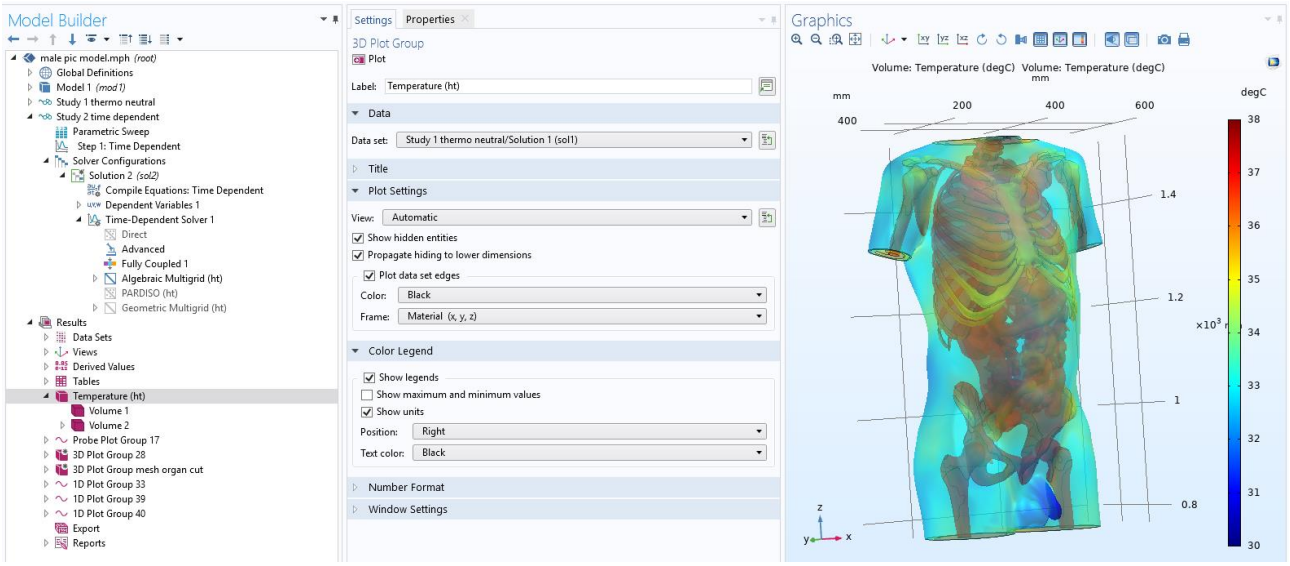

Figure 14: results 1 plotting

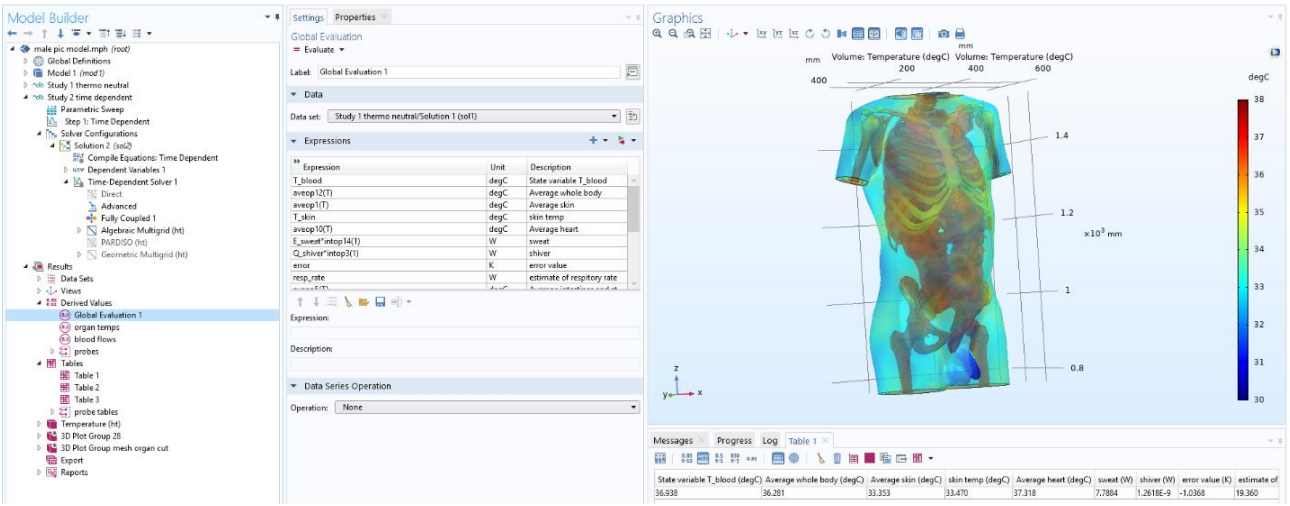

Figure 15: results 2 deriving values

PRIMITIVE VALIDATION

THERMAL NEUTRAL

An ambient temperature of 28°C, a wind speed of 0.4 $m \cdot s^{-1}$, and a relative humidity of 40% was defined as being thermal neutral. In the model, no thermoregulation occurs except insensible evaporative skin water loss in the steady state. This gave the basal values used for calculating the thermoregulation that occurs in other ambient conditions and the initial values for the dynamic simulations. Table 4 gives the thermal neutral values used throughout the simulations.

Table 4: thermal neutral organ values

variable	Temperature (°C)
T_{s_0}	33.35
T_{h_0}	37.31
T_{fat_0}	35.85
T_{muscle_0}	36.57
$T_{bladder_0}$	37.41
$T_{stomach_0}$	36.96
$T_{intestine_0}$	36.94
T_{kidney_0}	37.02
T_{lungs_0}	36.94
T_{liver_0}	37.12
T_{bones_0}	36.91

VALIDATION

Validations were performed by comparing simulations with published data from human testing. Overall the resulting temperatures of the simulations showed the same temperature profiles in the temperature vs. time plot as the results, but temperatures were usually higher in hot environments and the rectal temperature was colder during simulations in cold environments. Simulations were also not expected to yield exact results because only a torso is modeled and the exchange of heat between arms and legs with the environment is absent.

Simulation 1

The first simulation used the data reported in Stolwijk and Hardy [2] where subjects were in T_a of 30°C for 30 minutes followed by a T_a of 48°C for two hours before returning to T_a of 30°C for another hour. To run the simulation, a static simulation was performed where T_a was initially set to 28°C, the model's thermal neutral temperature.

Then, a dynamic simulation was performed where T_a started off at 28°C and increased to 30°C within the first two minutes and then increased to 48°C after 30 minutes and decreased back to 30°C after 150 minutes. The total simulation time was 210 minutes. The results of the simulation are shown in Figure 16 and Figure 17. No rectal region is defined in the model geometry. Multiple points were looked at such as the fat where the rectal region would be, the bladder, and the muscle surrounding the body. The point chosen to represent the rectal region is located on the interior surface of the muscle, in the approximate region of the rectum. The rectal temperature (T_r) from the torso model appears to overpredict the temperature reported in the data, but the shape of the plots appear to be similar. The heart temperature was also shown as an approximation to the esophageal temperature and to illustrate how the rectal temperature and the heart/esophageal temperature differ in value and shape of plots. The average skin temperature was overpredicted in the simulation, with a modestly faster recovery time course was simulated compared to that observed by Stolwijk and Hardy. It is believed that these over predictions in temperature are due to the model only being a torso model. As torso temperatures are greater than measured arm and leg temperatures. The sweat heat loss appears to increase similarly, but the peak sweat rate was observed to be 110 ($kcal \cdot m^{-2} \cdot h^{-1}$) and 180 ($kcal \cdot m^{-2} \cdot h^{-1}$) for the torso model and recovery time was longer.

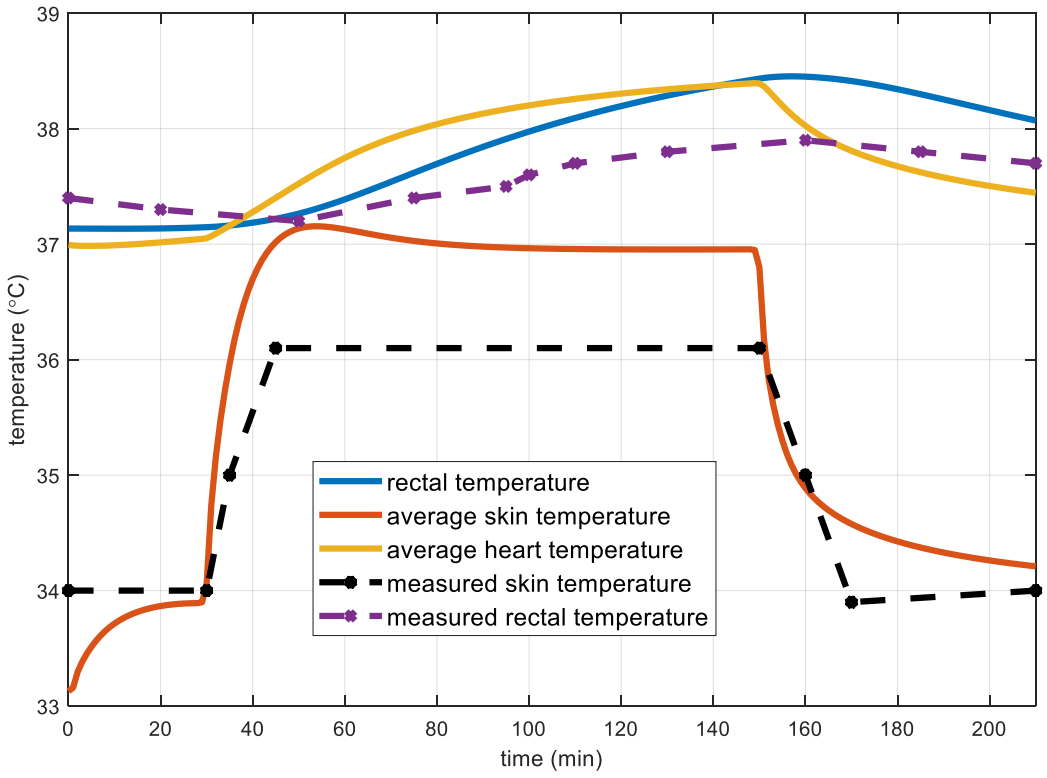

Figure 16: Measured and simulated core and skin temperatures

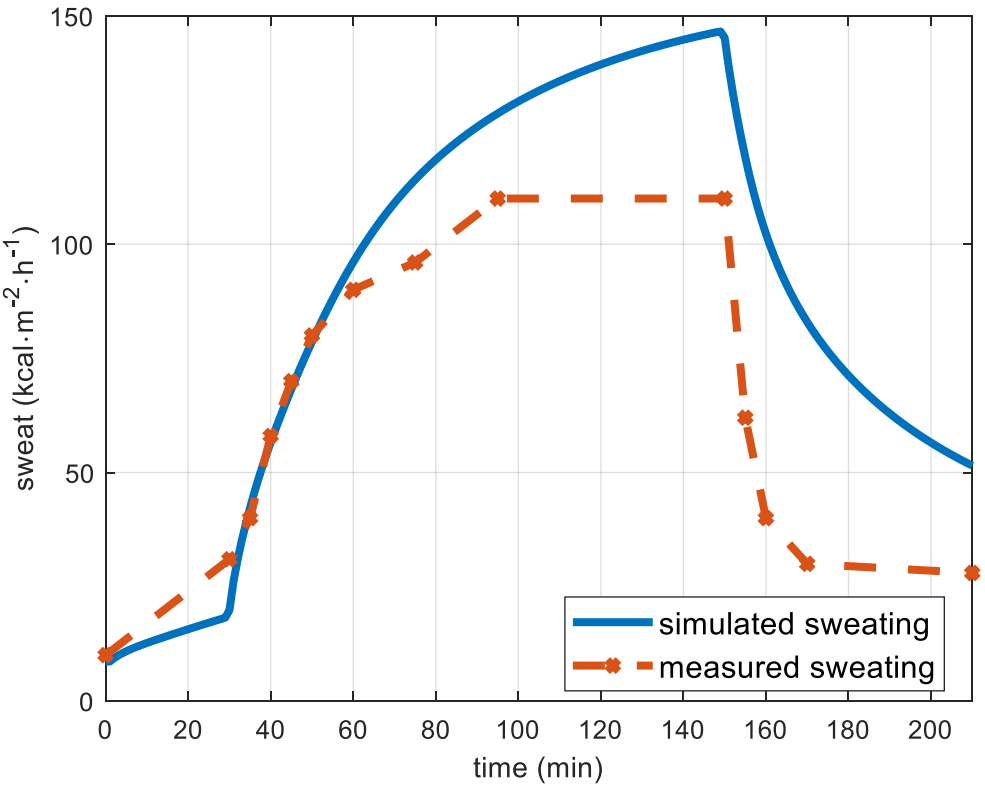

Figure 17: Measured and simulated heat loss due to sweat

Simulation 2

A second simulation was performed to examine thermal responses when T_a started at 28°C, was increased to 43°C immediately for 1 hour, decreased to 17°C for 2 hours and then set to 43°C again for another hour, as reported in Stolwijk and Hardy's report [2]. Figure 18 and Figure 19 show the results of the simulation with the torso model and the approximate data of Stolwijk and Hardy. When T_a = 43°C the predicted torso skin temperatures were about 1°C greater than observed in human skin and about 1°C warmer when T_a = 17°C. The rectal temperature in the simulation started at 37.1°C and rose to 37.6°C. Eventually the rectal temperature fell to 37.0°C. The subjects possessed initial rectal temperatures of approximately 37.2, which rose to approximately 37.4°C before decreasing to about 36.9°C when T_a = 17°C, but decreases further to about 36.6°C when T_a = 43°C before rising again. The heart temperature was used to approximate the esophageal temperature due to their adjacent locations. The predicted heart temperature increased ~0.2°C than the measured esophageal temperature, but the esophageal temperature fell with same approximate time course when T_a was set to 17°C. Sweating occurred during the simulations and evaporative heat loss and patterns followed the observed pattern when T_a was adjusted. In constrast, the simulation predicted a shivering response when T_a was lowered from 43C to 17C. No shivering was reported by Stolwijk and Hardy.

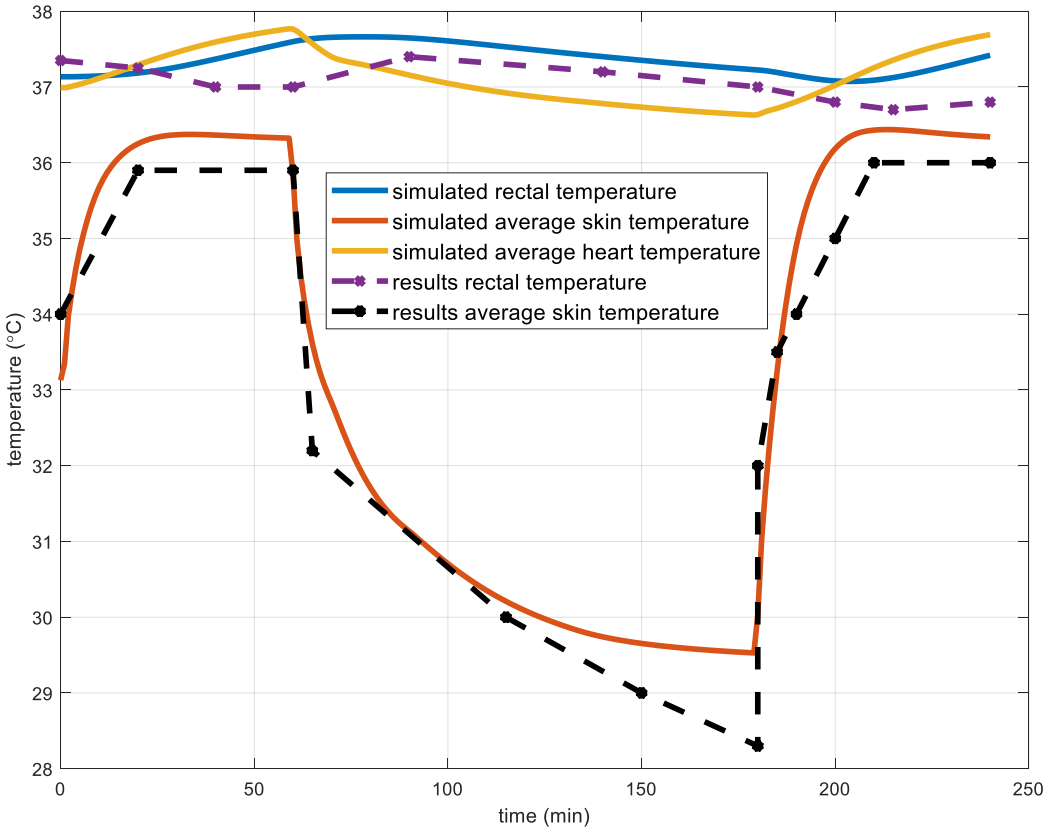

Figure 18: Measured and simulated temperatures of the rectum, heart, and skin

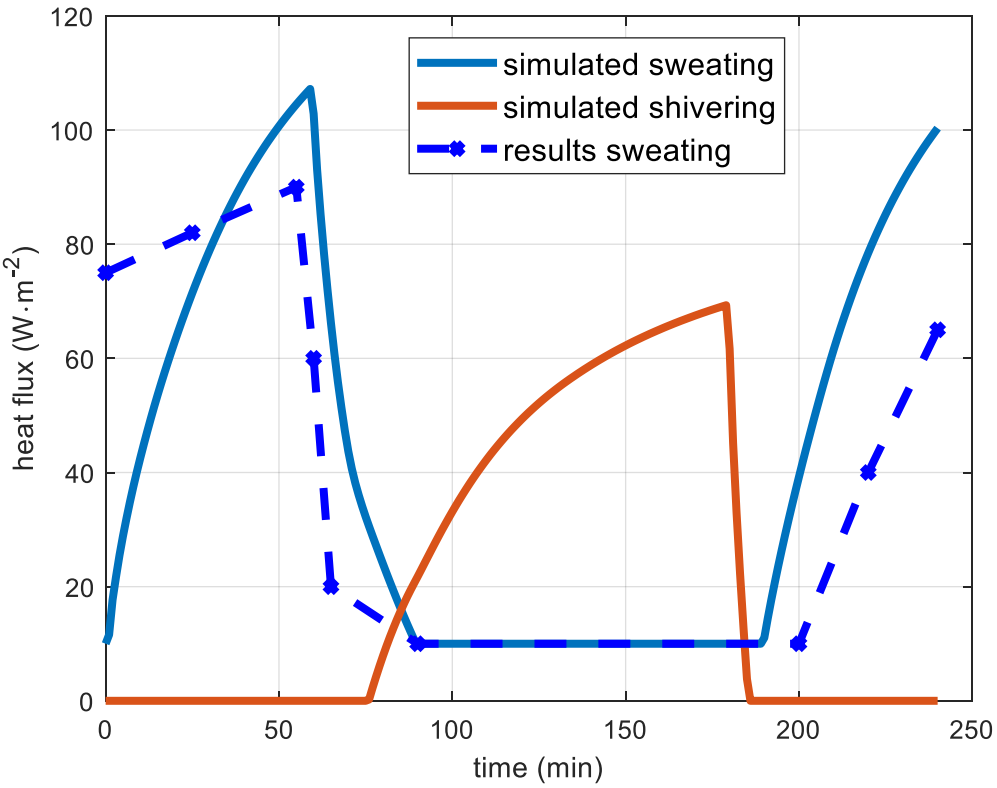

Figure 19: Measured and simulated sweating and shivering

Simulation 3

A third human simulation was performed where the ambient conditions were replicated from Bittel et al. [15], where subjects were initially in a room at a T_a of 30°C before the ambient temperature dropped to either 10, 5, or 1°C for 125 minutes (t = 0 corresponds to 5 minutes after the subjects enter the chamber). The results are shown in Figure 20, Figure 21, and Figure 22. Figure 20 shows the T_r from the simulation and the observed values. Both the simulation and the study show an initial increase in temperature, followed by a drop in the temperature. The predicted decline in torso core temperature was modeled more pronounced than what was observed. Whereas the model predicted a clear distribution of T_r; with highest defined T_r when T_a = 10°C and lowest when T_a = 1°C, this separation was less apparent in the supplemental data. Figure 21 illustrates the change in skin temperature. Both the simulation and results follow the same temperature profile. The simulated skin temperature appears to track the recorded skin temperature very well. In the simulation where T_a = 10°C the final skin temperature was 24.8°C in the simulation and approximately 24°C in the study. When T_a = 5°C, the final skin temperature was 22.4°C in the simulation and appears to be approximately 22.2°C in the study. When T_a = 1°C, the final skin temperature was 20.5°C in the simulation and approximately 20°C in the study. Figure 22 shows the results of shivering produced in $W \cdot m^{-2}$. The figure displaying the results shows the heat produced through shivering while the figure from the results shows the metabolic heat production of the entire body. Overall the results show that there is a change of 55 $W \cdot m^{-2}$ when T_a = 10°C, 92 $W \cdot m^{-2}$ when T_a = 5°C, and 110 $W \cdot m^{-2}$ when T_a = 1°C. The results from the study appear to show an initial increase that is greater than that of the simulation, but the amount of shivering at the end of the simulation is less than that of the simulation. While the heat measured from shivering is greater in the simulation most of the body shivering is in the torso, which would cause the heat produced to be higher per surface area.

Figure 23 and Figure 24 show cross sections of the torso throughout the first 30 minutes when T_a = 1°C. These cuts were an attempt to show the initial increase in rectal temperature, but the change is only about 0.2°C, which cannot be observed in the figures. However, they do show how the body cools in the first 30 minutes of the simulation.

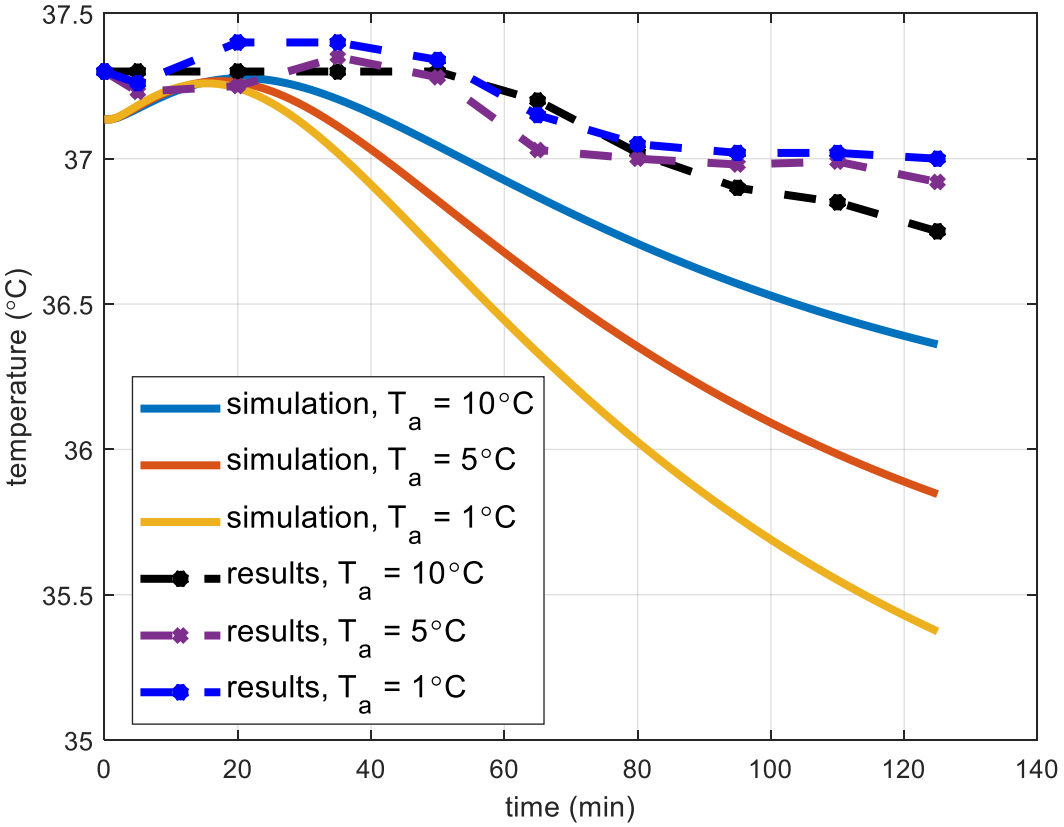

Figure 20: Simulated and measured rectal temperatures from the simulation (left) and from Bittel et al. [15] (right)

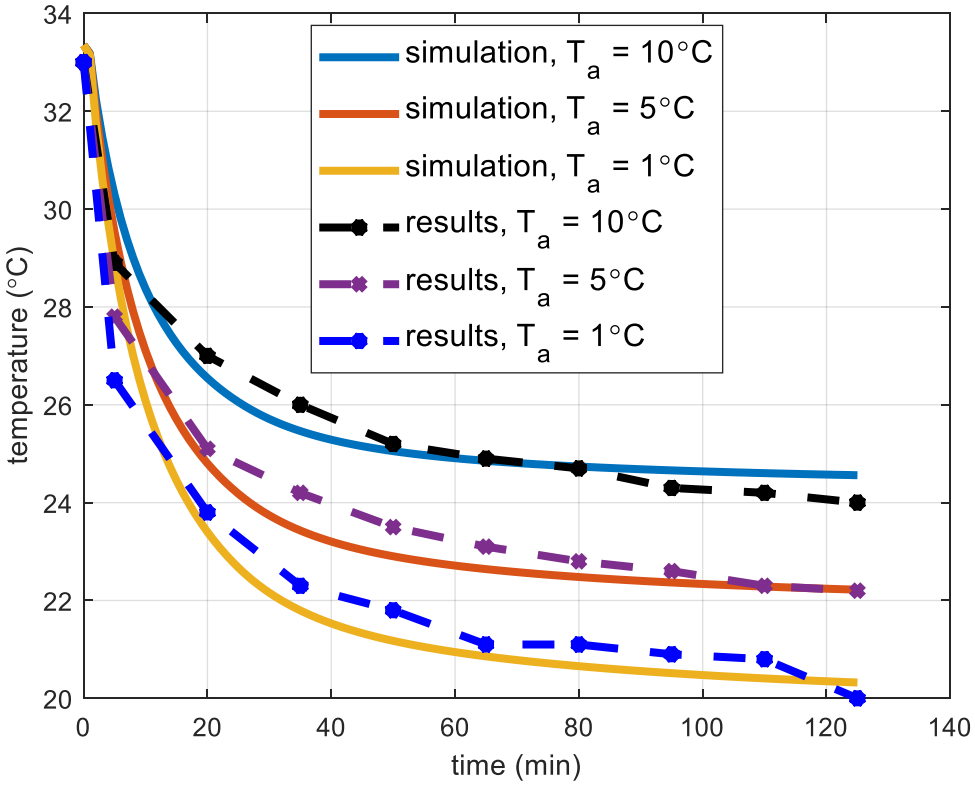

Figure 21: Simulated and measured skin temperatures

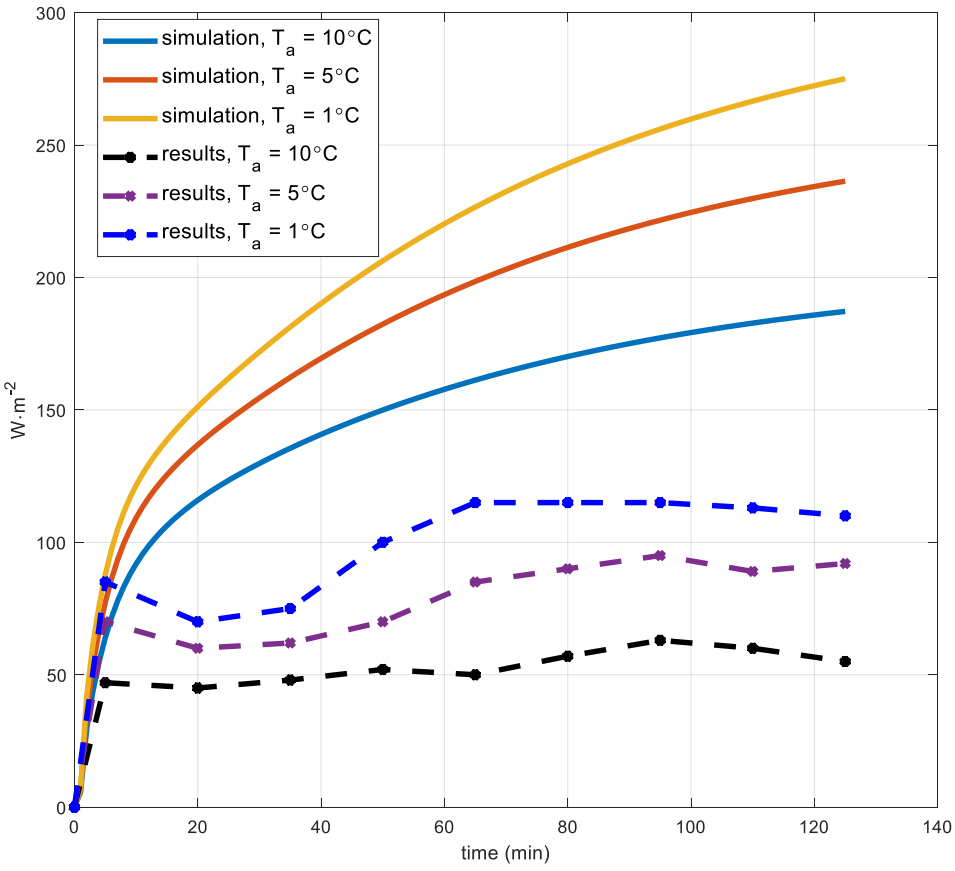

Figure 22: Simulated and measured shivering

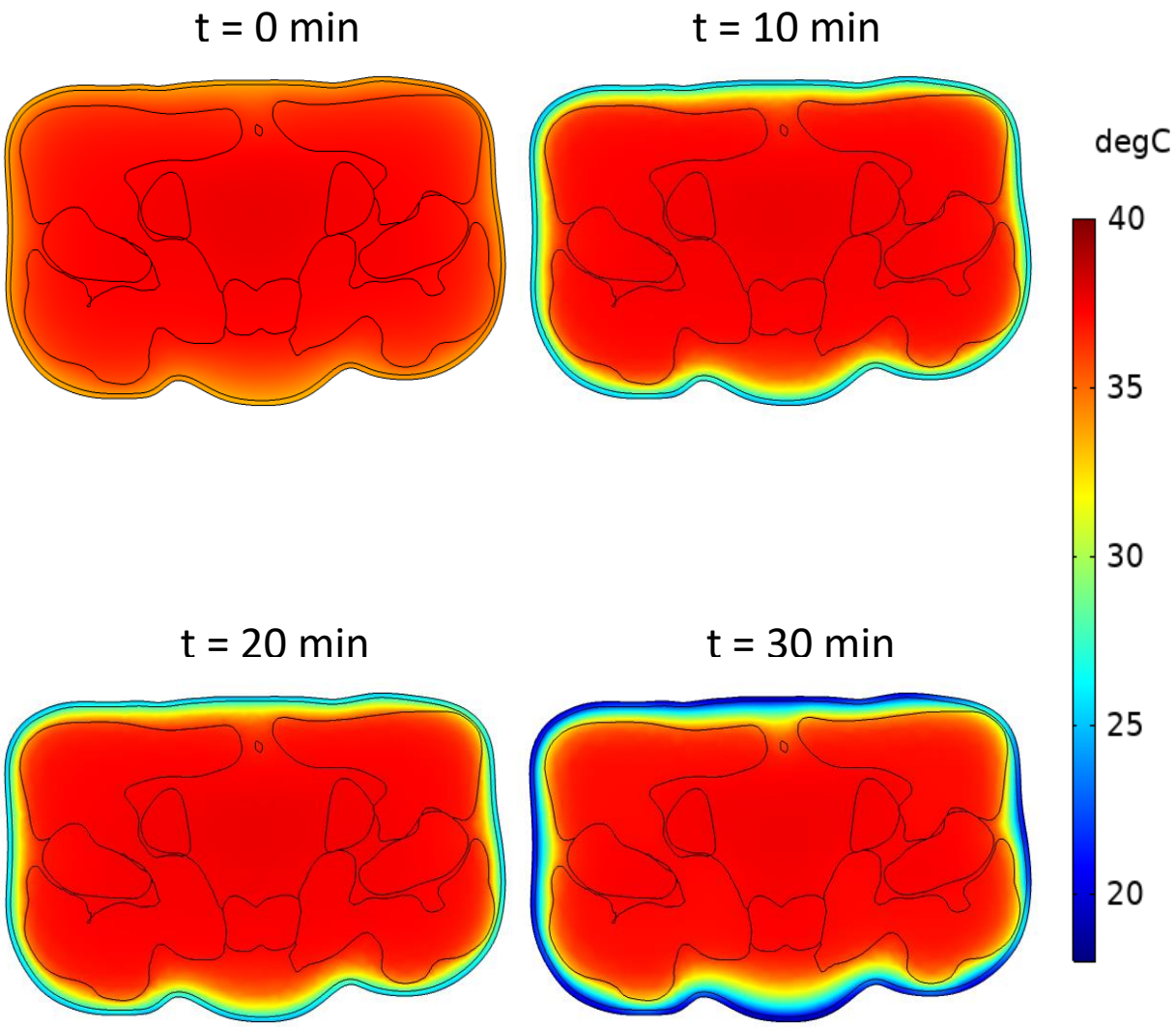

Figure 23: Temperature profiles at different times, T_a = 1°C

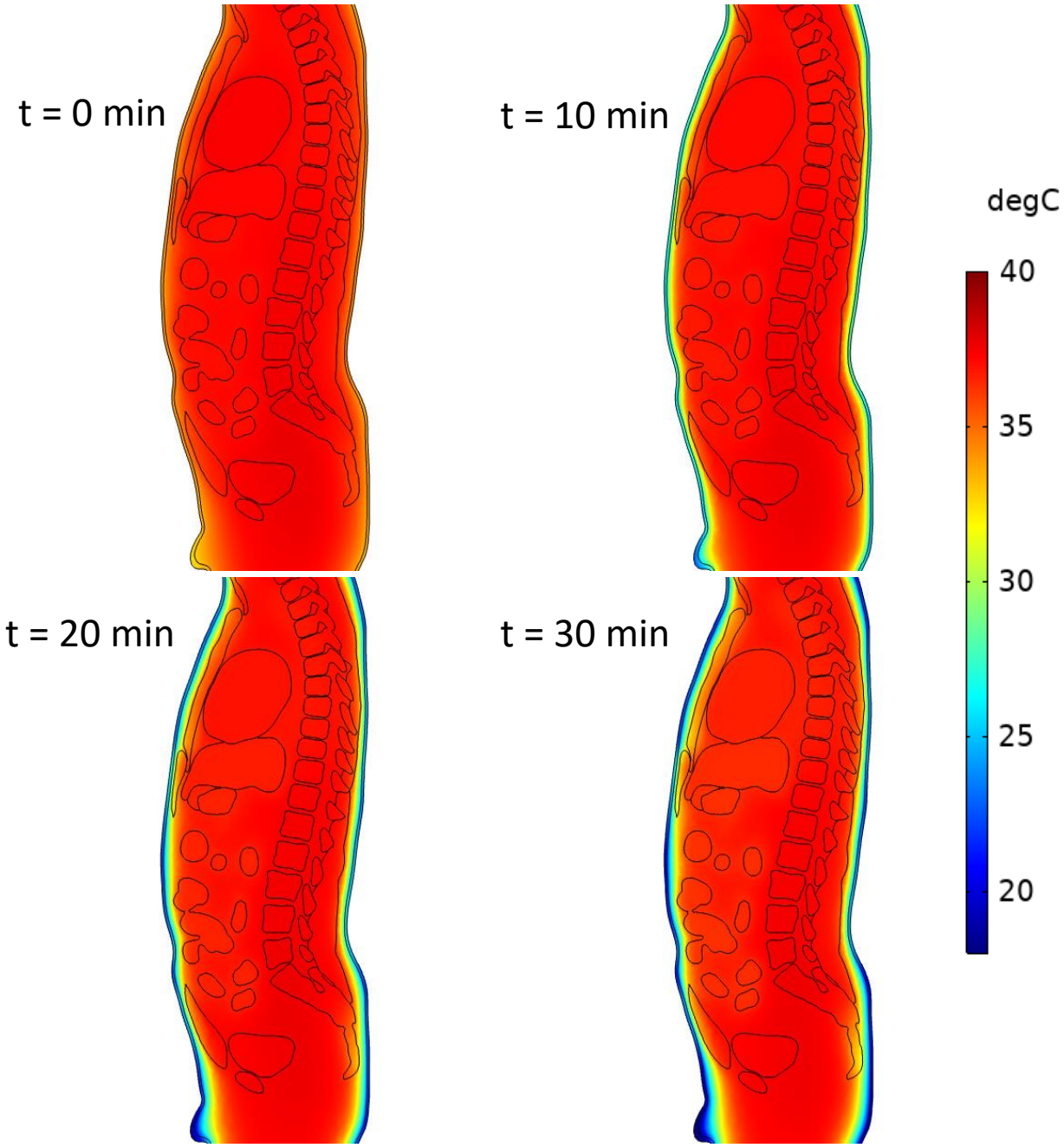

Figure 24:Simulated temperature profils at at different times, T_a = 1°C

DISCUSSION

VALIDATIONS

The validations indicate that the model produced outcomes that generally agree with the measured responses although absolute values were not always in an agreement. Thus the finite element thermoregulatory model created from medical images and thermoregulatory principles appear to predict physiological responses with reasonable accuracy. There were more differences, however, as more shivering and sweating occurred per unit area in the simulations than in the literature. This is expected to be because the torso has a surface of 0.78 m^2, while a typical male has a BSA of around 2 m^2.

APPLICATIONS

This model provides features that traditional simple geometry based thermoregulatory models cannot. For example, the model can be used to understand differences in core temperature measured at discrete locations. As shown in Figure 16, the core temperature measured in the esophagus (heart temperature) and in the rectum were different when the subjects were moved from 48°C to 28°C environments.

The intestinal temperature can be measured throughout any simulation and visualized as in Figure 25. It shows a maximum intestinal temperature of 37.1°C and a minimum of 36.2°C. This is a similar to observed values by Goodman et al. [16] where they showed a difference of 0.8°C between two temperature pills ingested at different times. This difference can be important when trying to accurately measure the core temperature. Figure 25 illustrates how the position of the intestine affects its temperature. The closer it is to the surface, the colder it appears.

The model could be used to map heat transfer within the body and to the skin surface. Figure 26 illustrates how heat is transferred to the skin internally in Simulation 1, Simulation 2, and Simulation 3. In the thermal neutral environment, 43 W are transferred to the skin by conduction compared to 13 by the blood convection. When placed in a warm enough environment, the heat transfer by conduction decreases and the heat transfer by the blood convection increases due to vasodilation, eventually surpassing the heat from conduction. When in a cold environment, the heat transfer by blood convection decreases due to vasoconstriction and heat transfer by conduction increases due to increases in temperature differences between the body and environment. Thus the model captures the roles of heat transfer by blood convection and by conduction.

The model can also be used to calculate the average body temperature. The scientific definition of mean body temperature is the average temperature of all the tissues in the body. The true average body temperature is defined as

$$T_b = p_1 T_1 + p_2 T_2 + p_3 T_3 + \cdots \quad \text{Eq. 29}$$

where T_b is the average body temperature (°C), $p_1, p_2, p_3, \ldots$ are the percentages of each tissue in the body (decimal), and $T_1, T_2, T_3, \ldots$ are the average temperatures of each tissue (°C). With this finite element torso model, it is possible to calculate the scientifically correct mean body temperature. In practice, only the core and skin temperatures are measured. Thus, Burton proposed an approach to estimate the average body temperature with the skin temperature an internal measurement such that [17]

$$T_b = \beta_1 T_{in} + (1 - \beta_1) T_s \quad \text{Eq. 30}$$

Here T_b is the average body temperature (°C), T_{in} is the internal body temperature (°C), T_s is the average skin temperature (°C), and β_1 is a constant such that $0 \leq \beta_1 \leq 1$. Burton proposed $\beta_1 = 0.8$. The results from Simulation 1, Simulation 2, and Simulation 3 (ambient temperatures ranging from 1 to 48°C) were combined to calculate the optimal value for β_1. The estimated T_r was used as the T_{in}. The optimal value for β_1 was calculated to be 0.81. Figure 27 shows the actual vs. predicted mean body temperature and the residual plot. The red line corresponds to $y = x$. Some have proposed to add a constant in calculating the average body temperature [18]. If one fits a linear model the model becomes

$$T_b = -0.871 + 0.840 T_r + 0.181 T_s \quad \text{Eq. 31}$$

Both slopes are significant ($p \approx 0$) and the intercept is significant with $p = 0.015$. This model produces an $r^2 = 0.992$. Figure 28 shows the actual and predicted value of the linear model and its residual plot. There does not appear to be much difference between the two plots, but the residual plot shows a slight improvement when the constant is added.

Another application of this model is creating temperature cuts like Figure 23 and Figure 24 under Simulation 3 and Figure 25 below. This can allow researchers to view what is happening inside the body. Animations of dynamic simulations can be made to aid in the visualization. This could also be a tool used in teaching thermoregulation and human physiology.

In addition, this model can be potentially used to evaluate performance or effectiveness of personal heat or cooling systems. Other models cannot accurately represent systems with non-uniform boundary conditions due to their simplicities. Systems that require advanced modeling include personal cooling systems, force air warming cover system, body armor covering the torso [19-22], and local arm heating systems covering just the forearm [23]. This model has the capabilities to create boundary conditions necessary to accurately represent these systems and will generate more accurate results.

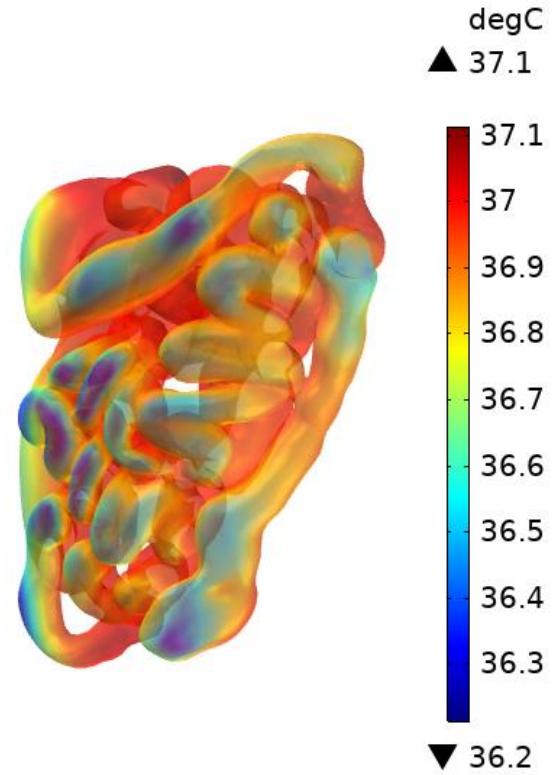

Figure 25: Intestinal temperature at thermal neutral conditions

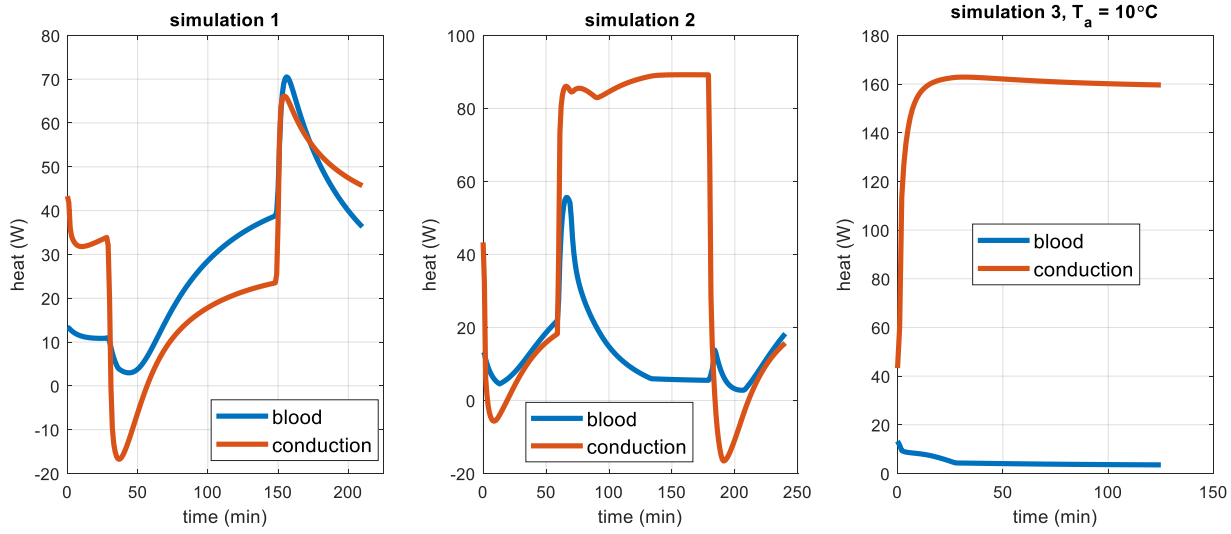

Figure 26: heat transfer to skin by conduction and blood for simulation 1 (left), simulation 2 (right), and simulation 3 (right)

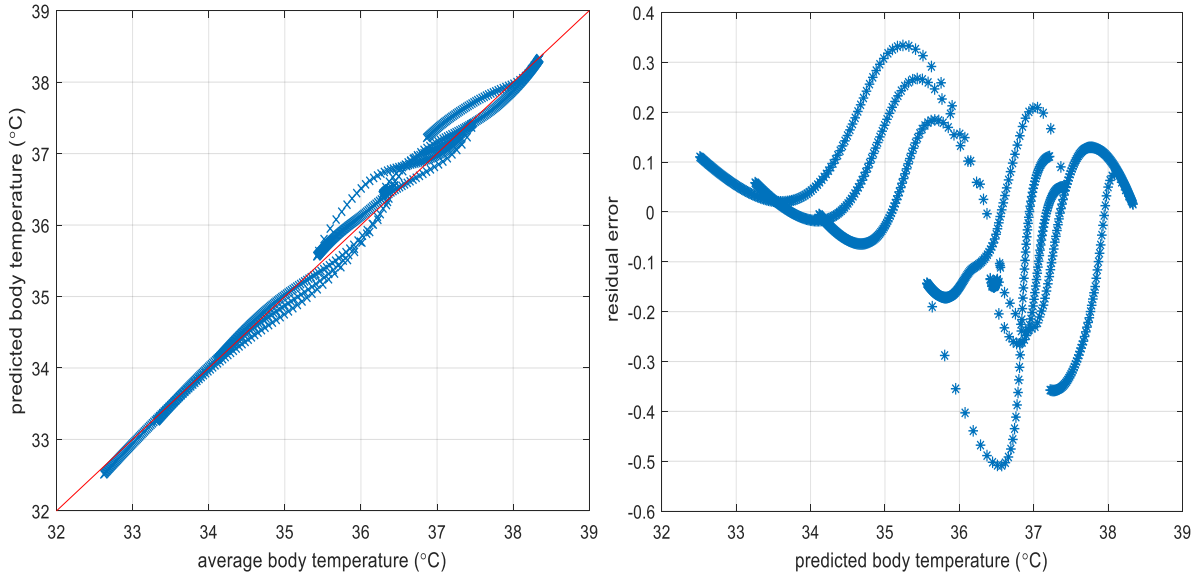

Figure 27: actual vs. predicted mean body temperature of $T_b = 0.81T_{re} + 0.19T_s$ (left) and its residual plot (right)

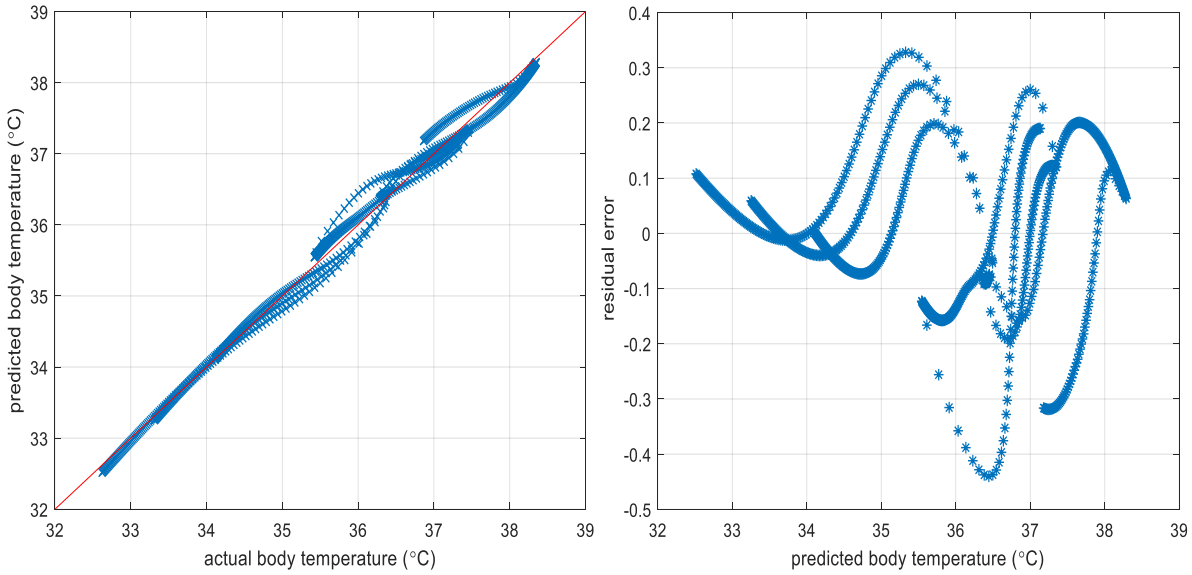

Figure 28: actual vs. predicted mean torso temperature of $T_b = -0.871 + 0.840T_{re} + 0.181T_s$ (left) and its residual plot (right)

POTENTIAL IMPROVEMENTS

The model can be improved by adding or creating the entire body. This would enable heat transfer across the entire skin surface and across the torso, legs, arms, and head. The torso has a body surface area (BSA) of 0.78 m^2, however, a typical male has a BSA of approximately 2 m^2. This implies only about 39% of the true surface area of the male torso is exchanging heat with the environment in the torso model. In scaling up to a whole body model, the geometry can be improved to include more detail in the hip/rectal region. This way more reliable rectal temperatures should be possible. A second improvement would be to apply the model to female anatomy or develop a way to transform the mesh to fit a female torso. These added capabilities would allow for closer examination of heat transfer within the geometry of human anatomy.

CONCLUSIONS

This paper introduces a thermoregulation model of the human body created using finite element analysis and a medical image based torso model. The methods described here are an improvement over past thermoregulatory modeling because the geometry is based off of medical image data, while older models used cylinders and CAD models. The advantage of using medical image data is that modeling is performed with anatomically correct organs, tissue, and body geometry, whereas cylinder models rely on an inner layer representing the core, followed by layers of muscle, fat, and skin. This causes the temperatures of the rectum and heart/esophagus to be approximately the same and follow the same temperature profile. With the new model the temperature curves of the heart/esophagus and the rectal temperature more closely follow observed responses to changing in heat production and flux. This project proves that the finite element combined with method and medical image based humans can be successfully used to model human physiological responses to changing ambient temperatures. The next step is to expand this approach to a whole-body model and develop a thermoregulatory finite element method model for the whole-body.

REFERENCES

1. Xu, X. and P. Tikuisis, *Thermoregulatory modeling for cold stress.* Compr Physiol, 2014. **4**(3): p. 1057-81.

2. Stolwijk, J.A. and J.D. Hardy, *Control of body temperature.* Comprehensive Physiology, 2010: p. 45-68.

3. Wissler, E.H., *Steady-state temperature distribution in man.* J. Appl. Physiol, 1961. **16**: p. 734-740.

4. Xu, X. and J. Werner, *A dynamic model of the human/clothing/environment-system.* Appl. Human Sci, 1997. **16**(2): p. 61-75.

5. Xu, X., P. Tikuisis, and G. Giesbrecht, *A mathematical model for human brain cooling during cold-water near-drowning.* J. Appl. Physiol, 1999. **86**(1): p. 265-272.

6. Kraning II, K.K. and R.R. Gonzalez, *A mechanistic computer simulation of human work in heat that accounts for physical and physiological effects of clothing, aerobic fitness, and progressive dehydration.* J Therm Biol, 1997. **22**(4-5): p. 331-342.

7. ASHRAE, A.H., *Fundamentals, American Society of Heating.* Refrigeration and Air-conditioning Engineers, Atlanta, GA, USA, 1997.

8. Stolwijk, J.A., *A mathematical model of physiological temperature regulation in man.* 1971.

9. Kenefick, R.W., S.N. Cheuvront, and M.N. Sawka, *Thermoregulatory function during the marathon.* Sports medicine, 2007. **37**(4-5): p. 312-315.

10. Fregly, M. and C. Blatteis, *Handbook of Physiology. Environmental Physiology Section 4*. Vol. 1. 1996.

11. Xu, X., et al., *Thermoregulatory model for prediction of long-term cold exposure.* Computers in biology and medicine, 2005. **35**(4): p. 287-298.

12. Bell, D.G., P. Tikuisis, and I. Jacobs, *Relative intensity of muscular contraction during shivering.* J Appl Physiol (1985), 1992. **72**(6): p. 2336-42.

13. Eyolfson, D.A., et al., *Measurement and prediction of peak shivering intensity in humans.* European journal of applied physiology, 2001. **84**(1-2): p. 100-106.

14. Xu, X. and J. Werner, *A dynamic model of the human/clothing/environment-system.* Applied human science, 2001. **16**(2): p. 61-75.

15. Bittel, J., et al., *Physical fitness and thermoregulatory reactions in a cold environment in men.* Journal of Applied Physiology, 1988. **65**(5): p. 1984-1989.

16. Goodman, D.A., et al., *Influence of sensor ingestion timing on consistency of temperature measures*. 2009, ARMY RESEARCH INST OF ENVIRONMENTAL MEDICINE NATICK MA THERMAL AND MOUNTAIN ….

17. Burton, A.C., *Human Calorimetry: II. The Average Temperature of the Tissues of the Body: Three Figures.* The Journal of Nutrition, 1935. **9**(3): p. 261-280.

18. Kenny, G.P. and O. Jay, *Thermometry, calorimetry, and mean body temperature during heat stress.* Compr Physiol, 2013. **3**(4): p. 1689-719.

19. Xu, X., *Optimierung des Systems Mensch/Kuhlanzug bei Hitzearbeit*. 1996, Clausthal-Zellerfeld: Papierfliege.

20. Xu, X., et al., *Efficiency of liquid cooling garments: prediction and manikin measurement.* Aviat. Space Environ. Med, 2006. **77**(6): p. 644-648.

21. Giesbrecht, G.G., P. Pachu, and X. Xu, *Design and evaluation of a portable rigid forced-air warming cover for prehospital transport of cold patients.* Aviation, space, and environmental medicine, 1998. **69**(12): p. 1200-1203.

22. Potter, A.W., et al., *Biophysical Assessment and Predicted Thermophysiologic Effects of Body Armor.* PLoS. One, 2015. **10**(7): p. e0132698.

23. Castellani, J.W., et al., *The effect of localized microclimate heating on peripheral skin temperatures and manual dexterity during cold exposure.* J Appl Physiol (1985), 2018.